AFOSR Scientific Report AFOSR 65-1907
ASRL TR 131-1

THEORETICAL CONSIDERATIONS OF PANEL FLUTTER AT HIGH SUPERSONIC MACH NUMBERS

John Dugundji

MASSACHUSETTS INSTITUTE OF TECHNOLOGY
AEROELASTIC AND STRUCTURES RESEARCH LABORATORY

August 1965

AIR FORCE OFFICE OF SCIENTIFIC RESEARCH
UNITED STATES AIR FORCE
CONTRACT NO. AF 49(638)-1528

AFOSR Scientific Report AFOSR 65-1907
ASRL TR 134-1

THEORETICAL CONSIDERATIONS OF PANEL FLUTTER AT HIGH SUPERSONIC MACH NUMBERS

John Dugundji

MASSACHUSETTS INSTITUTE OF TECHNOLOGY
AEROELASTIC AND STRUCTURES RESEARCH LABORATORY

August 1965

AIR FORCE OFFICE OF SCIENTIFIC RESEARCH
UNITED STATES AIR FORCE
CONTRACT NO. AF 49(638)-1528

ACKNOWLEDGEMENT

This report was made within the Aeroelastic and Structures Research Laboratory under United States Air Force Contract No. AF 49(638)-1528. The project is administered by Dr. J. Pomerantz of the Air Force Office of Scientific Research, United States Air Force.

The author wishes to acknowledge helpful discussions with Prof. Earl Dowell and the expert computational assistance of Mrs. Nancy Ghareeb. Also, the author would like to thank Miss Mary Campbell who prepared the figures, and Miss Judith Poole who typed the manuscript.

ABSTRACT

The general characteristics of panel flutter at high supersonic Mach numbers are examined theoretically. Linear plate theory and two-dimensional first order aerodynamics are used. The report attempts to clarify the important role of damping, the relationship between traveling and standing wave theories of panel flutter, and the effects of edge conditions. The solution procedures and general mathematical behavior may be of interest in other stability problems characterized by the appearance of complex eigenvalues.

TABLE OF CONTENTS

NOMENCLATURE

A	Coefficient of basic Eq. (18)
A.R.	Amplification ratio
a	Length of panel
B_R, B_I	Coefficients of basic Eq. (18)
b	Width of Panel
C	Coefficient of basic Eq. (18)
c	Wave speed
c_o	Reference wave speed = $1.90\ c_M\ h/b$
c_A, c_M	Speed of sound in air and in panel material
D	Plate rigidity = $Eh^3/12(1-\nu^2)$
E_n	Coefficient defined by Eq. (70)
f	Factor defined by Eq. (81)
G_s	Panel structural damping
g_A	Aerodynamic damping coefficient = $.335\left\{\frac{M(M^2-2)}{(M^2-1)^{3/2}}\right\}\frac{\rho_A}{\rho_M}\frac{c_A}{c_M}\left(\frac{a}{h}\right)^2$
g_s	Effective structural damping coefficient = $g_i\frac{\omega_i}{\omega_o}$
g_T	Total damping coefficient = $g_A + g_s$
g_i	Actual structural damping coefficient of i^{th} mode $\approx 2 \times$ (critical damping ratio)
H_m	Coefficients
h	Thickness of panel
i	$\sqrt{-1}$
K	Elastic foundation stiffness
k	Foundation parameter = $Ka^4/\pi^4 D$

ℓ	Wavelength
M	Mach number
m	Number of half waves in lateral direction
N_x, N_y	Longitudinal and lateral compressive forces
Δp_A	Aerodynamic pressure loading
Q_R, Q_I	Coefficients defined by Eqs. (28a,b)
q_n	Generalized coordinate of n^{th} mode
r_x	Longit. compression parameter = $N_x a^2/\pi^2 D$
r_y	Lateral compression parameter = $N_y a^2/\pi^2 D$
S	Parameter defined by Eq. (54)
t	Time
U	Velocity
$w, \bar{w}$	Deflection of panel
x,y	Coordinates along length and width
z_m	Roots of characteristic equation of Eq. (18)
$\bar{\alpha}$	Decay rate = $R_e\{\bar{\theta}\}$
Δ	Determinant defined by Eq. (24)
η	Nondimensional coordinate = y/b
$\bar{\theta}$	Response of system = $\bar{\alpha} + i\bar{\omega}$
λ	Dynamic pressure parameter = $\rho_A U^2 a^3/D\sqrt{M^2-1}$
ν	Poisson's ratio $\approx .3$
ξ	Nondimensional coordinate = x/a
ρ_A, ρ_M	Density of air and of panel material
τ	Nondimensional time = $\omega_o t$

Φ	Complex function defined by Eq. (25)
ψ	Effective structural damping ratio = $\frac{g_2 \omega_2}{g_1 \omega_1}$
ω	Frequency
ω_o	Reference frequency = $\pi^2 \sqrt{D/\rho_M h a^4}$
ω_i	Frequency of i^{th} mode
$\bar{\omega}$	Nondimensional frequency = ω/ω_o = $Im\{\bar{\theta}\}$

Subscripts

R	Real
I	Imaginary
F	Flutter
0	Reference

Superscripts

$\sim$	Corresponding nondimensional quantities for low aspect ratio panels (nondimensionalization based on b rather than on a).

SECTION I
INTRODUCTION

Panel flutter is the self-excited oscillation of the external skin of a flight vehicle when exposed to an airflow on one side.

This type of aeroelastic instability has received much study during the past fifteen years, both theoretically and experimentally. The early work of Sylvester and Baker,[1] Nelson and Cunningham,[2] Fung,[3] Hedgepeth,[4] Movchan,[5] Houbolt,[6] to mention a few names, has been supplemented by much recent work on the subject (see, for example, Refs. 7 through 14). Today, a great quantity of literature on panel flutter exists, and the problem is reasonably understood, although work still remains to be done to better correlate theory with experiment for certain panel configurations and Mach numbers. Fung,[10,15] in two excellent survey papers discusses the status of the panel flutter problem. See also, Dowell and Voss,[11] Bohon and Dixon,[14] Johns,[16] Kordes, Tuovila, and Guy,[17] and Shirk and Olsen.[18]

The present report will review the theoretical characteristics of panel flutter at high supersonic Mach numbers, and will attempt to clarify some of the loose ends in the literature regarding the role of damping, traveling-wave versus standing-wave theories, and effects of edge conditions. It is hoped thereby to clearly present the high Mach number panel flutter problem and its ramifications, some of which may not have been apparent heretofore.

The solution procedures and general mathematical behavior may be of interest also in other stability problems characterized by the appearance of complex eigenvalues.

SECTION II
BASIC PANEL FLUTTER EQUATION AND ITS SOLUTION

The basic panel flutter problem can be formulated by considering a flat, rectangular panel, simply supported on all four edges, and subjected to a supersonic flow over one side. See Fig. 1. The panel additionally is subjected to midplane compressive forces N_x and N_y (lbs/in), rests on an elastic foundation K (lb/in^3), and has a structural damping G_s ($lbs\text{-}sec/in^3$). The governing differential equation for this situation is,

$$D\left(\frac{\partial^4 w}{\partial x^4} + 2\frac{\partial^4 w}{\partial x^2 \partial y^2} + \frac{\partial^4 w}{\partial y^4}\right) = \Delta p_A - \rho_M h \frac{\partial^2 w}{\partial t^2} - N_x \frac{\partial^2 w}{\partial x^2} \quad (1)$$

$$- N_y \frac{\partial^2 w}{\partial y^2} - K w - G_s \frac{\partial w}{\partial t}$$

where D is the plate rigidity, Δp_A is the aerodynamic pressure, ρ_M is the density of the panel material, and h is the panel thickness.

The aerodynamic pressure for high supersonic Mach numbers ($M > 1.7$), can be reasonably described by the two-dimensional, first-order theory approximation,[3]

$$\Delta p_A \approx - \frac{\rho_A U^2}{\sqrt{M^2 - 1}} \left\{ \frac{\partial w}{\partial x} + \frac{M^2 - 2}{M^2 - 1} \frac{i}{U} \frac{\partial w}{\partial t} \right\} \quad (2)$$

This expression assumes the pressure on the bottom side remains constant at the free-stream value p_∞. Note also for large M, the above reduces to aerodynamic piston theory[19] since

$\sqrt{M^2-1} \longrightarrow M$ and $(M^2-2)/(M^2-1) \longrightarrow 1$.

Combining Eqs. (1) and (2), and introducing the nondimensional coordinates ξ , η , τ defined as

$$\xi = \frac{x}{a} \qquad \eta = \frac{y}{b} \qquad \tau = \omega_o t \tag{3}$$

will result in the basic partial differential equation for panel flutter,

$$\frac{\partial^4 w}{\partial \xi^4} + 2\left(\frac{a}{b}\right)^2 \frac{\partial^4 w}{\partial \xi^2 \partial \eta^2} + \left(\frac{a}{b}\right)^4 \frac{\partial^4 w}{\partial \eta^4} + \lambda \frac{\partial w}{\partial \xi} + \pi^4 g_T \frac{\partial w}{\partial \tau}$$
$$+ \pi^4 \frac{\partial^2 w}{\partial \tau^2} + \pi^4 k w + \pi^2 r_x \frac{\partial^2 w}{\partial \xi^2} + \pi^2 r_y \left(\frac{a}{b}\right)^2 \frac{\partial^2 w}{\partial \eta^2} = 0 \tag{4}$$

where the following nondimensional parameters have been introduced,

$$\lambda = \frac{\rho_A U^2 a^3}{D\sqrt{M^2-1}} \qquad \text{dynamic press. param.} \tag{5}$$

$$g_T = g_A + g_S \qquad \text{total damp. coeff.} \tag{6}$$

$$g_A = .335 \left\{\frac{M(M^2-2)}{(M^2-1)^{3/2}}\right\} \frac{\rho_A}{\rho_M} \frac{C_A}{C_M} \left(\frac{a}{h}\right)^2 \qquad \text{aero. damp. coeff.} \tag{7}$$

$$g_S = g_i \frac{\omega_i}{\omega_o} \qquad \text{effective struct. damp. coeff.} \tag{8}$$

a/b aspect ratio (9)

$$k = \frac{K a^4}{\pi^4 D} \qquad \text{foundation param.} \qquad (10)$$

$$r_x = \frac{N_x a^2}{\pi^2 D} \qquad \text{longit. compress. param.} \qquad (11)$$

$$r_y = \frac{N_y a^2}{\pi^2 D} \qquad \text{lateral compress. param.} \qquad (12)$$

In the above expressions, the reference frequency ω_o has been chosen as

$$\omega_o = \pi^2 \sqrt{\frac{D}{\rho_M h a^4}} \qquad (13)$$

which physically represents the lowest natural frequency of a two-dimensional simply-supported panel ($a/b \to 0$) with no airflow, elastic foundation, or midplane compressive forces present. Also, the total damping coefficient g_T is seen to be simply the sum of two parts, an aerodynamic damping coefficient g_A and an effective structural damping coefficient g_s . The aerodynamic damping coefficient g_A , first introduced by Houbolt,[6] ranges from 0 to 100 and is shown plotted in Fig. 2 for different panel sizes, altitudes, and panel materials.* This g_A is a more convenient parameter here, than the commonly used mass density parameter μ . The effective structural damping coefficient g_s is a consequence of the assumed constant structural damping G_s which can be expressed as,

$$G_s = g_i \omega_i \rho_M h \qquad (14)$$

*The Mach number factor in braces is often assumed to be its aerodynamic piston theory value of 1.

where $g_i = 2\zeta_i = 2\times$(critical damping ratio) of any mode ω_i . The form of Eq. (14) implies that for any other mode ω_j , the structural damping coefficient g_j will be given by $g_j = g_i \frac{\omega_i}{\omega_j}$. For typical panels, g_i ranges from 0 to 0.03 approximately. The consequences of using other values of g_j for the higher modes is explored in Section V.

Thus, the basic partial differential equation for panel flutter, Eq. (4), is seen to depend here on essentially six nondimensional parameters manely λ , g_T , a/b , ℓ_2 , r_x , r_y . This equation is to be solved subject to the simply-supported boundary conditions,

$$\text{at} \quad \xi = 0, 1 \longrightarrow \quad w = 0, \quad \frac{\partial^2 w}{\partial \xi^2} = 0 \qquad (15a)$$

$$\text{at} \quad \eta = 0, 1 \longrightarrow \quad w = 0, \quad \frac{\partial^2 w}{\partial \eta^2} = 0 \qquad (15b)$$

The solution procedure for Eq. (4) begins by seeking solutions in the form,

$$w(\xi, \eta, \tau) = \bar{w}(\xi) \left[\sin m\pi\eta \right] e^{\bar{\theta}\tau} \qquad (16)$$

where in general,

$$\bar{\theta} = \bar{\alpha} + i\bar{\omega} \qquad (17)$$

The η variation in Eq. (16) satisfies the boundary conditions at $\eta = 0, 1$. Unstable solutions will occur if $\bar{\theta}$ is real and positive (static instability) or complex with a positive real

part (dynamic instability). Inserting Eq. (16) into Eq. (4) will yield the ordinary differential equation,

$$\frac{d^4\bar{w}}{d\xi^4} + C\frac{d^2\bar{w}}{d\xi^2} + A\frac{d\bar{w}}{d\xi} + (B_R + iB_I)\bar{w} = 0 \tag{18}$$

where

$$C = \pi^2\left[-2\left(\frac{ma}{b}\right)^2 + r_x\right] \tag{19}$$

$$A = \lambda \tag{20}$$

$$B_R + iB_I = \pi^4\left[\left(\frac{ma}{b}\right)^4 + k - \left(\frac{ma}{b}\right)^2 r_y + g_T\bar{\theta} + \bar{\theta}^2\right] \tag{21}$$

To obtain a good insight into this problem, the basic ordinary differential equation, Eq. (18), subject to the boundary conditions, Eq. (15a), will first be solved thoroughly. Then, using Eqs. (19), (20), (21), the pertinent physical parameters λ, g_T, a/b, k, r_x, r_y, $\bar{\theta}$ will be related to the general coefficients C, A, B_R, B_I and physical panel flutter solutions will be obtained.*

*The mode parameter m is usually taken as $m = 1$. Actually all results come out in terms of ma/b which can be interpreted as an effective aspect ratio a/b' where $b' = b/m$.

The general solution of Eq. (18) is,

$$\bar{W}(\xi) = C_1 e^{z_1 \xi} + C_2 e^{z_2 \xi} + C_3 e^{z_3 \xi} + C_4 e^{z_4 \xi} \qquad (22)$$

where the C_m terms are arbitrary complex constants, and the z_m terms are the four roots of the complex characteristic equation of Eq. (18). Inserting $\bar{W}$ into the boundary conditions, Eq. (15a), yields the matrix equation,

$$\begin{bmatrix} 1 & 1 & 1 & 1 \\ z_1^2 & z_2^2 & z_3^2 & z_4^2 \\ e^{z_1} & e^{z_2} & e^{z_3} & e^{z_4} \\ z_1^2 e^{z_1} & z_2^2 e^{z_2} & z_3^2 e^{z_3} & z_4^2 e^{z_4} \end{bmatrix} \begin{Bmatrix} C_1 \\ C_2 \\ C_3 \\ C_4 \end{Bmatrix} = \begin{Bmatrix} 0 \\ 0 \\ 0 \\ 0 \end{Bmatrix} \qquad (23)$$

For nontrivial solutions of the constants C_m, the roots z_m must make the determinant Δ equal to zero, that is,

$$\Delta = \begin{vmatrix} 1 & 1 & 1 & 1 \\ z_1^2 & z_2^2 & z_3^2 & z_4^2 \\ e^{z_1} & e^{z_2} & e^{z_3} & e^{z_4} \\ z_1^2 e^{z_1} & z_2^2 e^{z_2} & z_3^2 e^{z_3} & z_4^2 e^{z_4} \end{vmatrix} = 0 \qquad (24)$$

For a given value of C and of A, various values of B_R and B_I can be selected, and the four roots z_1, z_2, z_3, z_4 of the complex characteristic equation of Eq. (18) can be found.

Then the complex function Φ can be evaluated, where *

$$\Phi = \frac{\Delta}{(z_1 - z_2)(z_1 - z_3)(z_1 - z_4)(z_2 - z_3)(z_2 - z_4)(z_3 - z_4)} \tag{25}$$

These values of $\Phi(B_R, B_I)$ can be plotted in the complex plane. The combination of B_R and B_I which makes $\Phi(B_R, B_I) = 0$ is a solution (eigenvalue) of Eqs. (18) and (15a) for the given C, A combination.

Equations (18) and (15a) were solved numerically by an IBM 1620 computer using the above procedure. Since many eigenvalues, B_R , B_I , can be found for each C, A combination, it was necessary to trace out continuously the proper eigenvalue branch by increasing A continuously from zero for a fixed value of C. It is to be noted that for A = 0, the eigenvalues are real $(B_I = 0)$, and are easily evaluated analytically from Eq. (18) as

$$B_R = -97.411\, n^4 + 9.8697\, n^2 C \tag{26}$$

where n is any integer. The eigenvalues remain real until a certain value of A is reached above which they become complex $(B_I \neq 0)$. Figures (3a-3c) show the real eigenvalues $(B_I = 0)$, while Figs. (4a-4c) show the complex eigenvalues. Only the most critical eigenvalue branches for this problem are

---

*The function Φ , rather than the determinant Δ itself, is evaluated to prevent the possibility of repeated roots causing the determinant to approach zero. Also, the function Φ , unlike the determinant Δ , will preserve its sign if one replaces z_1 by z_2 , etc.

indicated (largest B_I for a given C, A combination). Figure 5 indicates the minimum value of A for the first appearance of complex eigenvalues.

Returning to the physical panel flutter problem, it remains to relate the general coefficients C, A, B_R, B_I to the pertinent physical parameters λ, g_T, a/b, k, r_x, r_y, $\bar{\theta}$ of the problem. These relations are given by Eqs. (19), (20), and (21). Since $\bar{\theta}$ is to be determined for a given configuration, it is convenient to rewrite Eq. (21) as

$$\bar{\theta}^2 + g_T \bar{\theta} - (Q_R + i Q_I) = 0 \tag{27}$$

where,

$$Q_R = \frac{B_R}{\pi^4} + \left(\frac{ma}{b}\right)^2 r_y - \left(\frac{ma}{b}\right)^4 - k \tag{28a}$$

$$Q_I = \frac{B_I}{\pi^4} \tag{28b}$$

Equation (27) can be solved for $\bar{\theta}$ to give

$$\bar{\theta} = -\frac{g_T}{2} \pm \sqrt{\left(\frac{g_T}{2}\right)^2 + Q_R + i Q_I} \tag{29}$$

This can be further reduced to

$$\bar{\theta} = \left[-\frac{g_T}{2} + Re\{\Gamma\}\right] + i\left[Im\{\Gamma\}\right] \tag{30}$$

where

$$Re\{\Gamma\} = \pm\frac{1}{\sqrt{2}}\sqrt{+\sqrt{\left[\left(\frac{g_T}{2}\right)^2 + Q_R\right]^2 + \left[Q_I\right]^2} + \left(\frac{g_T}{2}\right)^2 + Q_R} \qquad (31a)$$

$$Im\{\Gamma\} = \frac{Q_I}{2\,Re\{\Gamma\}} \qquad (31b)$$

For a given configuration defined by given values of λ, g_T, a/b, k, r_x, r_y, Eqs. (19) and (20) can be used to find C and A. From the appropriate Figs. 3 and 4, values of B_R and B_I are found. Then Q_R and Q_I are evaluated from Eqs. (28a,b). Finally, $\bar{\theta} = \bar{\alpha} + i\,\bar{\omega}$ is solved from Eqs. (30) and (31a,b).

The complete panel behavior is characterized by plotting the $\bar{\alpha} + i\,\bar{\omega}$ variation with increasing dynamic pressure λ. Instability occurs when $\bar{\alpha}$ becomes positive (static type if also $\bar{\omega} = 0$, dynamic type if also $\bar{\omega} \neq 0$).

Some typical plots are shown in Fig. 6. For the case of no damping, $g_T = 0$, instability does not set in until after two undamped natural frequencies have merged (hence the common term "frequency coalescence flutter"). For some damping present $g_T > 0$, the instability sets in at a somewhat higher value of λ. This occurs when $\bar{\alpha} > 0$, i.e., when

$$-\frac{g_T}{2} + \frac{1}{\sqrt{2}}\sqrt{+\sqrt{\left[\left(\frac{g_T}{2}\right)^2 + Q_R\right]^2 + \left[Q_I\right]^2} + \left(\frac{g_T}{2}\right)^2 + Q_R} > 0 \qquad (32)$$

By routine algebraic manipulation, this criterion reduces to

$$\frac{Q_I}{\sqrt{-Q_R}} > g_T \qquad (33)$$

Hence flutter ($\bar{\alpha} = 0$) occurs when

$$\frac{Q_I}{\sqrt{-Q_R}} = g_T \tag{34}$$

At this flutter condition, it can be shown that $Re\{\Gamma\} = \pm \frac{g_T}{2}$, and thus the flutter frequency will be given by

$$\bar{\omega}_F = \sqrt{-Q_R} = \frac{\omega_F}{\omega_0} \tag{35}$$

Frequently, only the flutter condition is determined. However, the violence of the flutter can also readily be obtained from Eq. (30).

The deflection shape $W(\xi, \eta, \tau)$ for any physical situation is found by considering the real part of the right-hand side of Eq. (16). The complex function $\bar{W}(\xi)$ is given by Eq. (22) where the roots z_m are those for the given situation, and the complex constants c_m are found from Eq. (23). Setting $c_4 = 1$ and solving the first three equations of the matrix equation, Eq. (23), for c_1, c_2, c_3 gives

$$c_m = -\frac{N_m}{D} \qquad (m = 1, 2, 3) \tag{36}$$

where

$$\left.\begin{aligned} c_4 &= 1 \\ D &= \begin{vmatrix} 1 & 1 & 1 \\ z_1^2 & z_2^2 & z_3^2 \\ e^{z_1} & e^{z_2} & e^{z_3} \end{vmatrix} \end{aligned}\right\} \tag{37}$$

$$N_1 = \begin{vmatrix} 1 & 1 & 1 \\ z_4^2 & z_2^2 & z_3^2 \\ e^{z_4} & e^{z_2} & e^{z_3} \end{vmatrix}$$

$$N_2, N_3 = \text{etc.}$$

Then, taking the real part of the right-hand side of Eq. (16) gives

$$w(\xi,\eta,\tau) = \left[\sin m\pi\eta\right] e^{\bar{\alpha}\tau}\left(\bar{w}_R \cos\bar{\omega}\tau - \bar{w}_I \sin\bar{\omega}\tau\right) \tag{38}$$

This can be plotted for various times during one cycle ($\bar{\omega}\tau = 2\pi$) to give a clear physical picture of the deflection shape. At a flutter condition, one has $\bar{\alpha} = 0$ in the above equation. Some deflection shapes at flutter conditions ($\bar{\alpha} = 0$) are given in Figs. (7a-7ℓ) for various C,A combinations and the most critical eigenvalue branch (largest B_I for this given C, A combination), For $A = 0$, the deflection shapes are simple sine shape standing-wave types

$$w(\xi,\eta,\tau) = \left[\sin m\pi\eta\right] \sin n\pi\xi \cos\bar{\omega}\tau \tag{39}$$

As the coefficient A is increased for a fixed value of C, the deflection shape changes from a standing-wave type at low values of A where purely real eigenvalues ($B_I = 0$) are present, to a traveling-wave type at high values of A where complex eigenvalues ($B_I \neq 0$) are present. Also, the deflections tend to be concentrated at the rear end of the panel for large negative values of C. In these figures, only the first half of a period is shown since the second half is the negative of the first half.

The solution procedures used here for the panel flutter problem represent an exact solution rather than a modal solution of the differential equation and hence do not possess convergence difficulties. These procedures are analogous to those used previously by Dugundji and Ghareeb[20] for solving a related differential equation. See also Movchan[5,21].

Many other physical problems are characterized by the ordinary differential equation Eq. (18) subjected to boundary conditions Eq. (15a). The general solutions given by Figs. 3 to 5 and the mode shapes by Fig. 7 can be used to solve them also.

SECTION III
APPLICATIONS

The general theory presented in Section II is now applied to various physical panel configurations in order to show the characteristics of panel flutter and the effects of the six non-dimensional parameters, Eqs. 5 to 12. Essentially, the flutter condition ($\bar{\alpha} = 0$) will be examined, and plots of dynamic pressure parameter at flutter, λ_F, versus total damping coefficient, g_T, will be given for different a/b, k, r_x and r_y configurations. Also, an example of the complete panel behavior will be given.

(a) Pure Aspect Ratio Effects, a/b

For this series of panels, one considers $k = r_x = r_y = 0$, i.e., no elastic foundation, no longitudinal compression forces and no lateral compression forces present. For these cases, only dynamic type instability is possible. Figure 8 shows the dynamic pressure parameter at flutter λ_F, versus damping coefficient g_T for different aspect ratios a/b. The flutter dynamic pressure λ_F becomes large for low aspect ratios (high a/b). Also, λ_F becomes independent of damping g_T at low values of g_T and roughly proportional to g_T at high values of g_T. This indicates a change of panel flutter from a constant dynamic pressure phenomenon at low values of damping to a constant velocity phenomenon at high values of damping (thin, light panels in dense air). This also permits one to use the "static airforce approximation"[4], for $g_T < 1$.

The flutter frequencies $\bar{\omega}_F$ are also indicated in Fig. 8. The deflection mode shapes for the points marked with a heavy dot are given by Figs. 7a, b, c $\left(a/b = 0 \; ; \; \lambda_F = 370, \; 2000, \; 20{,}000\right)$,

Figs. 7e, f ($a/b = 4$; λ_F = 4,[illegible], [illegible]), and Fig. 7g [illegible] ; $\lambda_F = 60,000$). The modes are seen to change from standing wave types at low values of damping g_T to traveling wave types at high values of g_T. Also, the modes become of very short wave length, the deflections tend to be concentrated at the rear end, and the flutter frequency becomes high at large values of damping g_T and low aspect ratios (high a/b).

(b) Pure Elastic Foundation Effect, k

For this series of panels, one considers $a/b = r_x = r_y = 0$, i.e., two-dimensional panels with no longitudinal or lateral compression forces present. For these cases, again only dynamic instability is possible. Figure 9 shows λ_F versus g_T for different elastic foundation parameters k. The flutter dynamic pressure parameter λ_F increases with g_T and with k. The presence of some little damping g_T is very important at high values of k, since it can raise the flutter parameter λ_F well above the $g_T = 0$ value of $\lambda_F = 343$. Again, the flutter phenomena changes towards a constant velocity rather than a constant dynamic pressure phenomenon as g_T or k becomes large

The flutter frequencies $\bar{\omega}_F$ are also indicated in Fig. 9. At high values of k, the $\bar{\omega}_F$ becomes the simple natural frequency of the section mass-on-spring foundation. The deflection mode shapes for the points marked with a heavy dot are given by Figs. 7a, b, c (any value of k ; λ_F = 370, 2,000, 20,000). Again the modes change from standing wave types at low values of g_T and k to traveling wave types at high values of g_T and k. Also, the modes become of very short wave length, the deflections tend to be concentrated at the rear end, and the flutter frequency becomes high at large values of g_T and k.

(c) Pure Longitudinal Compression Effect, r_x

For this series of panels, one considers $a/b = k_2 = r_y = 0$, i.e., two-dimensional panels with no elastic foundation, and no lateral compressive forces present. Figure 10 shows λ_F versus g_T for different longitudinal compression forces r_x (negative r_x indicate tension forces). The dynamic pressure at flutter λ_F increases with increasing tension (negative r_x) and also with increasing damping g_T. Again the flutter phenomenon changes towards a constant velocity rather than a constant dynamic pressure phenomenon as g_T becomes large. For compressive forces $r_x > +1$, static instability may also occur. The nature of these curves for positive r_x is better illustrated by a cross plot, Fig. 11, which shows λ for instability plotted versus r_x . The regions of dynamic and static instability are readily apparent here. The point $\lambda = 0, r_x = 1$ represents the Euler buckling load of the panel. It is to be noted that aerodynamic forces may stabilize an otherwise statically unstable panel.

The flutter frequencies $\bar{\omega}_F$ are also indicated in Fig. 10. The deflection mode shapes for the points marked with a heavy dot are given by Figs. 7a, b, c ($r_x = 0$; $\lambda_F = 370, 2000, 20{,}000$), Figs. 7e, f ($r_x = -32$; $\lambda_F = 4600, 60{,}000$), and Fig. 7j ($r_x = +5$; $\lambda_F = 370$). Again the modes change from standing wave types at low values of g_T to traveling wave types at high values of g_T. Also, the modes become of very short wave length, the deflections tend to be concentrated at the rear end, and the flutter frequency becomes high at large values of g_T and negative r_x .

(d) Combined Compression and Aspect Ratio-Effects

For this series of panels, one considers $k_2 = 0$, i.e., no elastic foundation present, but with various combinations of the longitudinal compressive force r_x , lateral compressive force r_y

and aspect ratio a/b . For this category, two cases were considered, (a) r_x variable, $r_y = 0$, $a/b = 2$ and, (b) r_x variable, $r_y = r_x$, $a/b = 2$.

For Case (a), the results are shown in Figs. 12 and 13. The results are similar in nature to those given by Figs. 10 and 11, except that now a zero flutter dynamic pressure condition occurs at $r_x = +13$ which is before the onset of static instability at $r_x = +16$. This $\lambda_F = 0$ condition can readily be removed by addition of a small amount of damping g_T . In fact, it can be seen from Fig. 12 that this anomalous zero flutter dynamic pressure condition merely implies flutter occurs at a constant velocity rather than at a constant dynamic pressure here. The deflection mode shapes for the points marked with a heavy dot are given by Figs. 7a, b, c $(r_x = 8 \; ; \; \lambda_F = 370, 2000, 20{,}000)$, Figs. 7i, j $(r_x = 13; \; \lambda_F = 20, 370)$ and, Figs. 7k, l $(r_x = 18 \; ; \; \lambda_F = 200, 2000)$. The same general remarks as for the pure longitudinal compression effect described in Section IIIc apply here as well.

For Case (b) where $r_y = r_x$, the results are shown in Figs. 14 and 15. The results are similar in nature to those given by Figs. 10 and 11. Static instability sets in for $r_x > +5$. The deflection mode shapes for the points marked with a heavy dot are given by Figs. 7b, c $(r_x = 8 \; ; \; \lambda_F = 2000, \; 20{,}000)$. The same general remarks as for the pure longitudinal compression effect described in Section IIIc apply here as well.

(e) Boundary Support Effect

For this series of panels, one considers $k_e = r_x = r_y = 0$, i.e., no elastic foundation, no longitudinal or lateral compressive forces present, but with different aspect ratios and different boundary support conditions on the front and rear edges of the panel. For these cases, the basic Eq. 18 must be

solved again subject to the different boundary conditions present. Such calculations were performed for clamped-clamped panels by Movchan[22] and for clamped-free panels by Dugundji and Ghareeb[20]. The complex eigenvalues B_R, B_I for the clamped-clamped case as obtained by Movchan are presented in Fig. 16 along with the simply-supported ones used here for comparison. The resulting plots of dynamic pressure parameter at flutter λ_F versus damping g_T are shown in Fig. 17. In general, the clamped-clamped case gives a higher flutter dynamic pressure than the simply-supported case. However, at either low aspect ratios (high a/b) or at high values of damping g_T, the two λ_F's approach each other. This is probably due to the shorter wavelengths present in the flutter deflection shapes here, and hence a lesser influence of the end boundary conditions (see flutter deflection shape discussion in Section IIIa). Also shown for comparison is a clamped-free beam from results of Ref. 20. This also approaches the simply-supported case at high values of g_T where the mode shapes show short wavelength traveling waves present.

(f) Complete Panel Behavior

For interest, the series of panels examined in Section IIIa (Pure Aspect Ratio Effect) was re-investigated to give the complete panel behavior instead of merely the flutter condition.

For this series of panels, one has $\ell_2 = r_x = r_y = 0$. Then making use of the theory of Section II, the variation of $\bar{\theta} = \bar{\alpha} + i\bar{\omega}$ versus the dynamic pressure parameter $\hat{\lambda}$ was determined for different a/b and g_T configurations. Instead of plotting the $\bar{\alpha}$ and $\bar{\omega}$ versus λ, a new parameter, the amplification ratio, A.R., was introduced. This A.R. is defined as the ratio of amplitudes during one cycle of oscillation, and indicates the violence of flutter. It is given by

$$A.R. = e^{2\pi \frac{\bar{\alpha}}{\bar{\omega}}} \qquad (40)$$

Figure 18 shows the amplification ratio A.R. versus the dynamic pressure parameter λ , for $a/b = 0, 4$ and several values of g_T. Flutter (A.R > 1) is seen to set in very sharply for $a/b = 0$ and low values of damping g_T. For low aspect ratios $(a/b = 4)$ and also for high values of g_T, the flutter condition comes in more mildly. Also shown on this plot are some values of the frequency $\bar{\omega}$ associated with these amplification ratios.

SECTION IV
TRAVELING WAVE ANALYSIS

For low aspect ratio panels, the length along the stream direction is much larger than the width ($a/b >> 1$). One might consider such a panel as an infinitely long strip of finite width b, and seek traveling wave solutions of the basic partial differential equation.* Although the use of first order aerodynamics, Eq. 2, has certain limitations when applied to traveling waves[23], it will be used anyway in order to assess the differences between the traveling wave analysis and the finite panel analysis of the same mathematical equation.

The governing differential equations for panel flutter at high supersonic Mach numbers is given as before by Eqs. 1 and 2. Combining Eqs. 1 and 2, and introducing the new nondimensional coordinates $\tilde{\xi}$, η , $\tilde{\tau}$ defined as

$$\tilde{\xi} = \frac{x}{b} \qquad \eta = \frac{y}{b} \qquad \tilde{\tau} = \tilde{\omega}_o t \tag{41}$$

will result in the partial differential equation for panel flutter,

$$\frac{\partial^4 w}{\partial \tilde{\xi}^4} + 2\frac{\partial^4 w}{\partial \tilde{\xi}^2 \partial \eta^2} + \frac{\partial^4 w}{\partial \eta^4} + \lambda \frac{\partial w}{\partial \tilde{\xi}} + \pi^4 \tilde{g}_T \frac{\partial w}{\partial \tilde{\tau}}$$
$$+ \pi^4 \frac{\partial^2 w}{\partial \tilde{\tau}^2} + \pi^4 \tilde{\beta}_c w + \pi^2 \tilde{r}_x \frac{\partial^2 w}{\partial \tilde{\xi}^2} + \pi^2 \tilde{r}_y \frac{\partial^2 w}{\partial \eta^2} = 0 \tag{42}$$

---

*This traveling wave approach for low aspect ratio panels was investigated by Dowell (Ref. 23) using the complete linearized aerodynamic theory. Also, this traveling wave approach is often used in problems of cylindrical shell flutter (Ref. 10)

where the following new nondimensional parameters have been introduced,

$$\tilde{\lambda} = \frac{\rho_A U^2 b^3}{D\sqrt{M^2-1}} = \left(\frac{b}{a}\right)^3 \lambda \tag{43}$$

$$\tilde{g}_T = \tilde{g}_A + \tilde{g}_S = \left(\frac{b}{a}\right)^2 g_T \tag{44}$$

$$\tilde{g}_A = .335 \left\{\frac{M(M^2-2)}{(M^2-1)^{3/2}}\right\} \frac{\rho_A}{\rho_M} \frac{C_A}{C_M} \left(\frac{b}{h}\right)^2 = \left(\frac{b}{a}\right)^2 g_A \tag{45}$$

$$\tilde{g}_S = g_i \frac{\omega_i}{\tilde{\omega}_o} = \left(\frac{b}{a}\right)^2 g_S \tag{46}$$

$$\tilde{k} = \frac{K b^4}{\pi^4 D} = \left(\frac{b}{a}\right)^4 k \tag{47}$$

$$\tilde{r}_x = \frac{N_x b^2}{\pi^2 D} = \left(\frac{b}{a}\right)^2 r_x \tag{48}$$

$$\tilde{r}_y = \frac{N_y b^2}{\pi^2 D} = \left(\frac{b}{a}\right)^2 r_y \tag{49}$$

The above nondimensionalization, Eq. 41 and parameters Eqs. 43-49 are now based solely on the width b for this infinite traveling wave analysis. The reference frequency $\tilde{\omega}_o$ is here chosen as

$$\tilde{\omega}_o = \pi^2 \sqrt{\frac{D}{\rho_M h b^4}} \tag{50}$$

The basic partial differential equation, Eq. 42, is equivalent to the previous equation, Eq. 4.

The traveling wave solutions of Eq. 42 are sought in the form

$$\begin{aligned} w(\tilde{\xi}, \eta, \tilde{\tau}) &= w_o \left[\sin m\pi\eta\right] e^{i\frac{2\pi}{\ell}(ct - x)} \\ &= w_o \left[\sin m\pi\eta\right] e^{i\frac{2\pi}{\ell}\left(\frac{c}{\tilde{\omega}_o}\tilde{\tau} - b\tilde{\xi}\right)} \end{aligned} \tag{51}$$

where ℓ is the wavelength and c is the wavespeed which in general may be complex, i.e.,

$$c = c_R + i\, c_I \tag{52}$$

Generally, it is assumed that unstable solutions will occur if the wavespeed c has a negative imaginary part. The η variation in Eq. 51 satisfies the boundary conditions at $\eta = 0, 1$. Inserting Eq. 51 into Eq. 42 will yield the algebraic equation,

$$\left(\frac{c}{c_o}\right)^2 - i\,\frac{\tilde{g}_\tau \ell}{4b}\left(\frac{c}{c_o}\right) - S^2 + i\,\frac{\tilde{\lambda}\ell}{8\pi^3 b} = 0 \tag{53}$$

where

$$S = \frac{1}{2}\sqrt{m^4\left(\frac{\ell}{2b}\right)^2 + 2m^2 + \frac{1}{\left(\ell/2b\right)^2} + \left(\frac{\ell}{2b}\right)^2\tilde{k} - \tilde{r}_x - m^2\left(\frac{\ell}{2b}\right)^2\tilde{r}_y} \tag{54}$$

$$c_o = \frac{2b\tilde{\omega}_o}{\pi} = 1.90\,\frac{h}{b}\,c_M \qquad (55)$$

When no air forces and no structural damping are present, $\tilde{\lambda} = \tilde{g}_T = 0$, the above expression, Eq. 53 gives,

$$c = \pm S\,c_o \qquad (56)$$

For a panel with no spring foundation and no midplane compressive forces, $\tilde{k} = \tilde{r}_x = \tilde{r}_y = 0$, the minimum value of S occurs for $m = 1$ and $\ell/2b = 1$ and is given as $S_{min} = 1$. Hence, the reference wavespeed c_o can be interpreted physically above as the vacuum wavespeed for traveling waves with $m=1$, whose half wavelength, $\ell/2$, equals the width, b. This also happens to be the minimum vacuum wavespeed possible for such a panel. Note also the simple relation of c_o to the speed of sound in the material, c_M, Eq. 55.

Solving Eq. 53 for the wavespeed c in the presence of air forces and damping gives

$$\frac{c}{c_o} = i\,\frac{\tilde{g}_T \ell}{8b} \pm \sqrt{-\left(\frac{\tilde{g}_T \ell}{8b}\right)^2 + S^2 - i\,\frac{\tilde{\lambda}\ell}{8\pi^3 b}} \qquad (57)$$

This can be further reduced to

$$\frac{c}{c_o} = \left[Re\{\Gamma\}\right] + i\left[\frac{\tilde{g}_T \ell}{8b} + Im\{\Gamma\}\right] \qquad (58)$$

where

$$Re\{\Gamma\} = -\frac{\tilde{\lambda}\ell}{16\pi^3 b}\,\frac{1}{Im\{\Gamma\}} \tag{58a}$$

$$Im\{\Gamma\} = \pm\frac{1}{\sqrt{2}}\sqrt{+\sqrt{\left[S^2-\left(\frac{\tilde{q}_T\ell}{8b}\right)^2\right]^2+\left[\frac{\tilde{\lambda}\ell}{8\pi^3 b}\right]^2}-\left[S^2-\left(\frac{\tilde{q}_\pi\ell}{8b}\right)^2\right]} \tag{58b}$$

The complete panel behavior is characterized by plotting the $c_r + i\,c_I$ variation with increasing dynamic pressure $\tilde{\lambda}$ for various wavelengths $\ell/2b$. Instability is assumed to occur when c_I becomes negative. This occurs when

$$\frac{\tilde{q}_T\ell}{8b} - \frac{1}{\sqrt{2}}\sqrt{+\sqrt{\left[S^2-\left(\frac{\tilde{q}_T\ell}{8b}\right)^2\right]^2+\left[\frac{\tilde{\lambda}\ell}{8\pi^3 b}\right]^2}-\left[S^2-\left(\frac{\tilde{q}_\pi\ell}{8b}\right)^2\right]} < 0 \tag{60}$$

By routine algebraic manipulation, this criterion reduces to

$$\tilde{\lambda} > 2\pi^3 S\,\tilde{q}_T \tag{61}$$

Hence, flutter $(c_I = 0)$ occurs when

$$\tilde{\lambda} = 2\pi^3 S\,\tilde{q}_T \tag{62}$$

or equivalently,

$$U = 1.90\left(\frac{M^2-2}{M^2-1}\right) S\,\frac{h}{b}\,c_M \tag{63}$$

where S is a function mainly of wavelength ratio $\ell/2b$ as defined by Eq. 54. At the flutter condition, Eq. 59b yields $Im\{\sqrt{\ }\} = \pm \tilde{g}_T \ell / 8b$ and the corresponding wavespeed and frequency at flutter become,

$$c_F = + S\, c_o \tag{64}$$

$$\omega_F = \frac{2\pi}{\ell} S\, c_o = 2\left(\frac{2b}{\ell}\right) S\, \tilde{\omega}_o \tag{65}$$

For a panel with no spring foundation and no midplane compressive forces ($\tilde{k} = \tilde{r}_x = \tilde{r}_y = 0$), the minimum value of S is $S_{min} = 1$ and occurs for $m = 1$ and $\ell/2b = 1$. Placing these values of S and $\ell/2b$ into the above expressions, Eqs. 62-65 gives the condition for the first onset of flutter, for such panels.

Figure 19 shows a plot of the dynamic pressure parameter at flutter $\tilde{\lambda}_F$ versus the damping $\tilde{g}_T$ for the infinite panel traveling wave theory. Also shown for comparison are the results of the previously obtained finite panel analyses, Fig. 8, when converted to the parameters $\tilde{\lambda}_F$ and $\tilde{g}_T$ using Eqs. 43 and 44. The traveling wave analysis gives a lower flutter dynamic pressure than the finite panel analysis, particularly at low values of $\tilde{g}_T$. At the higher values of $\tilde{g}_T$, the agreement and trends are better between the two theories. The flutter frequencies $\omega_F/\tilde{\omega}_o$ are also indicated in Fig. 19 and the agreements are fair. The deflection mode shapes for the infinite panel, traveling wave analysis, are simple sine shaped traveling waves of wavelength $\ell = 2b$, traveling at a wavespeed $c = c_o$ and having a frequency $\omega_F = 2\tilde{\omega}_o$. The corresponding deflection mode shapes of the finite panel for the points marked by a heavy dot are given in Figs. 7e, f ($a/b = \infty$; $\tilde{g}_T = .04$, 6.0) and Figs. 7g, h ($a/b = 10$; $\tilde{g}_T = .036$, $.80$).

They clearly resemble traveling waves and are qualitatively similar in wavelength, wavespeed, and frequency to the infinite panel, particularly at high values of $\tilde{g}_T$. These finite panels though, show large deflection amplitudes towards the rear of the panel, as compared with the uniform deflection amplitudes of the infinite panel, traveling wave analysis. For convenience, a comparison of the mode shapes from the two analyses is shown in Fig. 20 for the $a/b = 10$, $\tilde{g}_T = .80$ case.

Summarizing, it appears that an approximate idea of the flutter speed, frequency, wavespeed, and wavelength can be obtained from an infinite panel, traveling wave analysis for long, narrow panels at high values of damping $\tilde{g}_T$ (light, thin panels in dense air). However, the end effects still play important roles for panels of $a/b = 10$, and any accurate estimation of the flutter characteristics and deflection shapes should be made by finite panel analyses.

SECTION V
EFFECT OF ARBITRARY STRUCTURAL DAMPING

All of the preceding analyses have assumed that the actual structural damping coefficient g_j, of any mode ω_j was related to that of the fundamental mode ω_1 by the relation,

$$g_j = g_1 \frac{\omega_1}{\omega_j} \tag{66}$$

Other relationships may be assumed or measured experimentally. For example, the alternate relationship,

$$g_j = g_1 \tag{67}$$

is commonly employed in standard V-g flutter analyses in industry. It is of interest to examine the effect and sensitivity of these other g_j variations on the previous results.

To study these effects, it is convenient to solve the panel flutter problem by modal methods. The basic partial diffential equation of panel flutter is given by Eq. (4). Modal solutions of Eq. (4) are sought in the form,

$$w(\xi, \eta, \tau) = \sum_{n=1}^{N} q_n(\tau) \sin n\pi\xi \sin m\pi\eta \tag{68}$$

where $q_n(\tau)$ is the generalized coordinate of the n^{th} mode, and the mode shape, $\sin n\pi\xi \sin m\pi\eta$, satisfies the simply supported boundary conditions Eqs. (15a,b) on all edges. Inserting Eq. (68) into Eq. (4), and applying Galerkin's method will result after some algebra, in the set of ordinary differential equations,

$$\frac{d^2 q_n}{d\tau^2} + g_\tau \frac{dq_n}{d\tau} + E_n q_n + \frac{\lambda}{\pi^4} \sum^{n+s=odd} \frac{4sn}{n^2-s^2} q_s = 0 \qquad (69)$$

$$n, s = 1, 2, \cdots N$$

where,

$$E_n = n^4 + 2\left(\frac{ma}{b}\right)^2 n^2 + \left(\frac{ma}{b}\right)^4 + k_2 + r_x n^2 + r_y \left(\frac{ma}{b}\right)^2 \qquad (70)$$

The summation above is taken over all the s terms for which n + s is an odd integer.

Consider now, for simplicity, a two mode analysis. The above set of equations become,

$$\frac{d^2 q_1}{d\tau^2} + g_\tau \frac{dq_1}{d\tau} + E_1 q_1 - \frac{8\lambda}{3\pi^4} q_2 = 0 \qquad (71a)$$

$$\frac{d^2 q_2}{d\tau^2} + f g_\tau \frac{dq_2}{d\tau} + E_2 q_2 + \frac{8\lambda}{3\pi^4} q_1 = 0 \qquad (71b)$$

In the second equation, an arbitrary factor f was introduced to permit the possibility of changing the amount of total damping g_τ of the second mode. To investigate stability, one sets

$$q_n(\tau) = q_n e^{\bar{\theta}\tau} \qquad (72)$$

The characteristic determinant of the above equations then becomes,

$$\begin{vmatrix} \left(\bar{\theta}^2 + g_T\bar{\theta} + E_1\right) & -\frac{8\lambda}{3\pi^4} \\ \frac{8\lambda}{3\pi^4} & \left(\bar{\theta}^2 + f g_T + E_2\right) \end{vmatrix} = 0 \qquad (73)$$

Upon expansion, this gives the characteristic equation,

$$\bar{\theta}^4 + H_3\bar{\theta}^3 + H_2\bar{\theta}^2 + H_1\bar{\theta} + H_0 = 0 \qquad (74)$$

where,

$$\begin{aligned} H_3 &= g_T(1+f) \\ H_2 &= E_1 + E_2 + f g_T^2 \\ H_1 &= g_T\left(E_2 + f E_1\right) \\ H_0 &= E_1 E_2 + \left(\frac{8\lambda}{3\pi^4}\right)^2 \end{aligned} \qquad (75)$$

The roots $\bar{\theta} = \bar{\alpha} + i\bar{\omega}$ of Eq. (74) are examined as λ increases from zero for any fixed configuration. This gives the complete panel behavior. Instability occurs when $\bar{\alpha}$ becomes positive.

To investigate only the flutter condition $\bar{\alpha} = 0$, one sets $\bar{\theta} = i\,\omega_F$ in Eq. (74). This equation then splits into a real and an imaginary part, namely,

$$\bar{\omega}_F^4 - \left[E_1 + E_2 + f g_T^2\right] \bar{\omega}_F^2 + \left[E_1 E_2 + \left(\frac{8\lambda}{3\pi^4}\right)^2\right] = 0 \qquad (76a)$$

$$-g_T(1+f)\,\bar{\omega}_F^3 + g_T(E_2 + f E_1)\,\bar{\omega}_F = 0 \qquad (76b)$$

Solving Eq. (76b) gives the flutter frequency,

$$\bar{\omega}_F = \frac{\omega_F}{\omega_0} = \sqrt{\frac{E_2 + f E_1}{1+f}} \qquad (77)$$

Placing this into Eq. (76a) gives, after much algebra, the dynamic pressure parameter at flutter λ_F as

$$\lambda_F = 18.26\left(\frac{2\sqrt{f}}{1+f}\right)\sqrt{(E_2 - E_1)^2 + g_T^2(E_2 + f E_1)(1+f)} \qquad (78)$$

Equation (78) permits one to investigate the effect of unequal total damping ($f \neq 1$) on the flutter characteristics. A similar such equation was presented by Bolotin.[9]

Returning to the damping characteristics, it is recalled that the total damping is the sum of an aerodynamic damping g_A and an effective structural damping g_s. It is convenient now to differentiate between the damping in each mode, namely

$$g_{T1} = g_A + g_{s1} \equiv g_T$$
$$g_{T2} = g_A + g_{s2} \equiv f g_T \qquad (79)$$

where the effective structural damping coefficient g_{si} of the the i^{th} mode is given from Eq. (8) as

$$g_{si} = g_i \frac{\omega_i}{\omega_o} \tag{80}$$

The aerodynamic damping coefficient g_A remains the same for all modes and hence there is no need to differentiate here between the modes in Eq. (79). Using Eqs. (79) and (80), one may express the factor f as

$$f = \frac{g_{T2}}{g_{T1}} = \frac{1 + (g_{s1}/g_A)}{1 + \psi (g_{s1}/g_A)} \tag{81}$$

Thus, f is seen to depend on two nondimensional ratios, namely,

$$g_{s1}/g_A = \frac{g_1}{g_A} \frac{\omega_1}{\omega_o} \tag{82}$$

$$\psi = \frac{g_{s2}}{g_{s1}} = \frac{g_2}{g_1} \frac{\omega_2}{\omega_1} \tag{83}$$

Also, for interest, the total damping and the undamped natural frequencies of this two mode system can be expressed as,

$$g_T \equiv g_{T1} = g_A \left(1 + g_{s1}/g_A\right) \tag{84}$$

$$\frac{\omega_i}{\omega_o} = \sqrt{E_i} \tag{85}$$

For any combination of g_A, g_1, g_2 the ratios g_{s1}/g_A and Ψ may be evaluated from Eqs. (82), (83), and (85). The resulting values of f and g_T from Eqs. (81) and (84) may then be inserted into the two mode flutter formula Eq. (78) to obtain λ_F .

Figure 21 shows a plot of the factor f versus g_{s1}/g_A for various values of Ψ . Also shown on Fig. 21 is a plot of the important parameter $(2\sqrt{f}/1+f)$ versus f. For a given Ψ , as g_{s1}/g_A increases from zero, the value of f varies from $f = 1$ to the asymptotic value $f = 1/\Psi$. The corresponding value of $(2\sqrt{f}/1+f)$ decreases monotonically from unity to some other asymptotic value. Placing these results into the formula Eq. (78), one can see that because of the factor $(2\sqrt{f}/1+f)$, the addition of actual structural damping g_i may actually destabilize the system, particularly for systems where the aerodynamic damping g_A is small. The maximum amount of this destabilization possible depends solely on the effective structural damping ratio Ψ and is given from the asymptotic values of f as,

$$\frac{\lambda_F \text{ (with struct. damp.)}}{\lambda_F \text{ (no struct. damp.)}} \geq \frac{2\sqrt{\Psi}}{1+\Psi} \tag{86}$$

In the case of equal effective structural damping coefficients, $\Psi = 1$, the system is always stabilized by the addition of actual structural damping g_i.*

---

*This destabilization occurring upon the addition of damping has been pointed out by Ziegler[24], Bolotin[9], Johns[16] and others.

The previous theory was applied to a panel with $a/b = k = r_x = r_y = 0$, i.e., a two dimensional panel with no elastic foundation, and no longitudinal or lateral compressive forces present. For this case, $\omega_1/\omega_0 = 1$, and $\omega_2/\omega_0 = 4$. Two types of structural damping relationships were considered, namely a) $g_2 = g_1$ for which $\psi = 4$, and b) $g_2 = \frac{1}{4} g_1$ for which $\psi = 1$ (equal effective structural damping coefficients). Figure 22 shows the dynamic pressure parameter at flutter λ_F plotted versus the actual structural damping g_1 present in the panel, for these two cases at different values of aerodynamic damping. It is seen that at $g_A = .1$, the addition of actual structural damping $g_1 = .05$ will reduce the flutter dynamic pressure parameter from $\lambda_F = 274$ to $\lambda_F = 258$ for the $g_2 = g_1$ case, while there is a slight increase for the $g_2 = \frac{1}{4} g_1$ case. At $g_A = 1$, the destabilization for the $g_2 = g_1$ case is much less while again there is a slight increase in the $g_2 = \frac{1}{4} g_1$ case. These curves of λ_F versus g_1 clearly illustrate the typical "looping back" of the V-g curves of the standard flutter analysis used in industry. This "looping back" is thus seen to be a result of unequal effective structural damping coefficients, and not something associated with the use of viscous type damping rather than $ig\,k\,x$ type damping.*

To conclude this discussion, it might be interesting to give a simplified expression for the flutter parameter λ_F based on the two mode approximation, Eq. (78). If $E_1 \ll E_2$ and $g_T \ll 1$ Eq. (78) reduces simply to

---

*It is to be noted that for no aerodynamic or structural damping ($g_T = 0$), the dynamic pressure parameter at flutter $\lambda_F = 274$ for these two mode analyses rather than the exact value of $\lambda_F = 343$. A four mode analysis should actually be done for numerical accuracy. Figure 22 however does give the proper trends.

$$\lambda_F \approx 18.26 \left(\frac{2\sqrt{f}}{1+f}\right)(E_2 - E_1) \qquad (87)$$

This expression shows the direct relationship of the flutter parameter λ_F on the factor $(2\sqrt{f}/1+f)$, and was first given by Bolotin.[9] However, the crucial role of the effective structural damping ratio ψ in establishing the correct value of f to be used in this expression must clearly be understood (see Fig. 21).

SECTION VI
CONCLUSIONS

This report has reviewed the theoretical characteristics of panel flutter at high supersonic Mach numbers. By using linear plate theory and two-dimensional, first order aerodynamics, the problem was shown to depend on six nondimensional parameters, λ , g_T , a/b , k_2 , r_x , r_y .

An exact solution of the resulting partial differential equations revealed the nature of the eigenvalues and their general behavior. From these eigenvalues, both static and dynamic instabilities can be physically obtained. The solution procedure eliminates difficulties associated with convergence of modal methods and may also be of interest in other similar type stability problems, for example, wing flutter, flowing pipe lines, beam buckling, etc.

For understanding panel flutter, the effect of damping is important. At low values of g_T, panel flutter occurs at constant dynamic pressure q, and has the appearance of standing waves. At high values of g_T (light, thin panels in dense air), panel flutter occurs at constant velocity V, and has the appearance of traveling waves. Many analyses have been done previously assuming $g_T = 0$ (the "static air force approximation"). This is adequate in some ranges, but inadequate in others, particularly if $\lambda = 0$. This $\lambda = 0$ condition merely implies flutter occurs at constant velocity V, rather than at constant dynamic pressure q and does not mean the system is unstable for any airspeed.

For pure aspect ratio and pure elastic foundation, only dynamic type instabilities are possible, but with compressive forces r_x , r_y present, static type instabilities (buckling) can also occur.

The effects of front and rear edge conditions on the plate tend to become unimportant for low aspect ratios and also for high aerodynamic damping g_T, where the resulting mode shapes begin to appear like traveling waves.

The flutter condition appears to set in sharply for two-dimensional panels at low values of damping g_T . For low aspect ratios and for high values of g_T , the flutter condition comes in more mildly.

Infinite panel, traveling wave analysis can be used to obtain an approximate idea of the flutter characteristics of low aspect ratio panels at high values of damping g_T . The traveling wave analysis gives lower flutter speeds than the finite panel analysis and the details of the deflection mode shapes are somewhat different, but the general trends are similar

The effect of adding structural damping g_i to a finite panel is frequently destabilizing. The amount of this destabilization depends on the relative amount of structural damping added to each mode of the panel, and is characterized primarily by the ratio ψ . Limits on the maximum possible destabilization are established for a two mode analysis. If the effective structural damping is added equally ($\psi = 1$), the system is always stabilized.

REFERENCES

1. Sylvester, M.A., and Baker, J.E., Some Experimental Studies of Panel Flutter at Mach Number 1.3, NACA TN 3914, February 1957 (First published December 1952).

2. Nelson, H.C., and Cunningham, H.J., Theoretical Investigation of Flutter of Two-Dimensional Flat Panels With One Surface Exposed to Supersonic Flow, NACA TR 1280, 1956 (First published April 1955).

3. Fung, Y.C., On Two-Dimensional Panel Flutter, Journal of Aeronautical Sciences, Vol. 25, pp. 145-160, March 1958.

4. Hedgepeth, J.M., Flutter of Rectangular Simply Supported Panels at High Supersonic Speeds, Journal of Aeronautical Sciences, Vol. 24, pp. 563-573, August 1957.

5. Movchan, A.A., On Vibrations of a Plate Moving in a Gas, NASA Republ. 11-22-58 W, January 1959 (Translated from Prikl. Mat. Mekh., Vol 20, pp. 211-222, 1956).

6. Houbolt, J.C., A Study of Several Aerothermoelastic Problems of Aircraft Structures, Doctoral Thesis, E.T.H., Zurich, 1958.

7. Guy, L.D. and Dixon, S.C., A Critical Review of Experiment and Theory for Flutter of Aerodynamically Heated Panels, Symposium on Dynamics of Manned Lifting Planetary Entry, Philadelphia, Pa., October 1962, pp. 568-595, John Wiley & Sons, Inc., New York, New York, 1963.

8. Voss, H.M., The Effect of an External Supersonic Flow on the Vibrations of Thin Cylindrical Shells, Journal of Aerospace Sciences, Vol 28, pp. 945-956, December 1961.

9. Bolotin, V.V., Nonconservative Problems of the Theory of Elastic Stability, Macmillan Co., New York, New York, 1963 (Translation of original volume in Russian, 1961).

10. Fung, Y.C., Some Recent Contributions to Panel Flutter Research, AIAA Journal, Vol. 1, pp. 898-909, April 1963.

11. Dowell, E.H., and Voss, H.M., Experimental and Theoretical Panel Flutter Studies in the Mach Number Range 1.0 to 5.0, AIAA Paper 64-491, presented at the First Annual AIAA Meeting, Washington, D.C., June 1964.

12. Fralich, R.W., Postbuckling Effects on the Flutter of Simply Supported Rectangular Panels at Supersonic Speeds, NASA TN D-1615, March 1963.

13. Cunningham, H.J., Analysis of the Flutter of Flat Rectangular Panels on the Basis of Exact Three-Dimensional, Linearized Supersonic Potential Flow, AIAA Journal, Vol. 1, pp. 1795-1801, August 1963.

14. Bohon, H.L., and Dixon, S.C., Some Recent Developments in Flutter of Flat Panels, Journal of Aircraft, Vol. 1, pp. 280 - 288, September - October 1964.

15. Fung, Y.C., A Summary of the Theories and Experiments on Panel Flutter, AFOSR TN 60-224, Guggenheim Aeronautical Laboratory, California Institute of Technology, May 1960.

16. Johns, D.J., A Review of Panel Flutter at Low Supersonic Speeds, NPL Aero. Rept. 1102, A.R.C. 25 881, 0.1834, National Physical Laboratory, England, April 1964.

17. Kordes, E.E., Tuovila, W.J., Guy, L.D., Flutter Research on Skin Panels, NASA TN D-451, September 1960.

18. Shirk, M.H., and Olsen, J.J., Recent Panel Flutter Research and Applications, AGARD Report 475, September 1963.

19. Ashley, H. and Zartarian, G., Piston Theory - A New Aerodynamic Tool for the Aeroelastician, Journal of Aeronautical Sciences, Vol. 23, pp. 1109 - 1118, December 1956.

20. Dugundji, J. and Ghareeb, N., Pure Bending Flutter of a Swept Wing in a High-Density, Low Speed Flow, AIAA Journal, Vol. 3, pp. 1126 - 1133, June 1965.

21. Movchan, A.I., and Movchan, A.A., Traveling Waves in the Supersonic Flutter Problem of Panels of Finite Length, Proceedings of the International Council of Aero. Sciences, Third Congress, Stockholm, pp. 723 - 735, 1962, published by Spartan Books, Inc., Washington, D.C., 1964.

22. Movchan, A.A., Behavior of Complex Eigenvalues in the Problem of Panel Flutter, Academy of Sciences of the U.S.S.R., Institute of Mechanics, Inzh. Sbornik, Vol. 27, 1960.

23. Dowell, Earl, The Flutter of Very Low Aspect Ratio Panels, AFOSR 64-1723, Aeroelastic and Structures Research Laboratory TR 112-2, Massachusetts Institute of Technology, July 1964.

24. Ziegler, H., On the Concept of Elastic Stability, Advances in Applied Mechanics, Vol 4, Academic Press Inc., New York, New York, pp. 351 - 403, 1956.

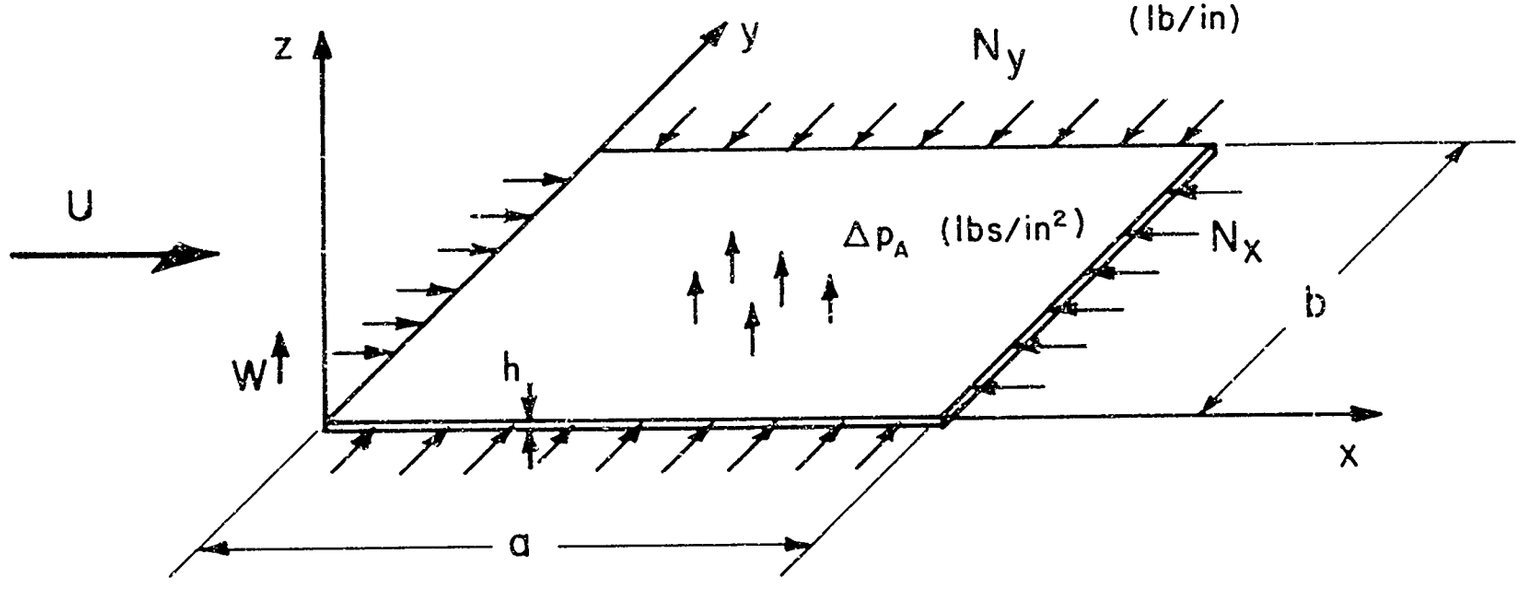

Also, panel rests on elastic foundation K (lbs/in^3)
panel has viscous structural damping G_s (lbs-sec/in^3)

FIG. 1 BASIC PANEL CONFIGURATION

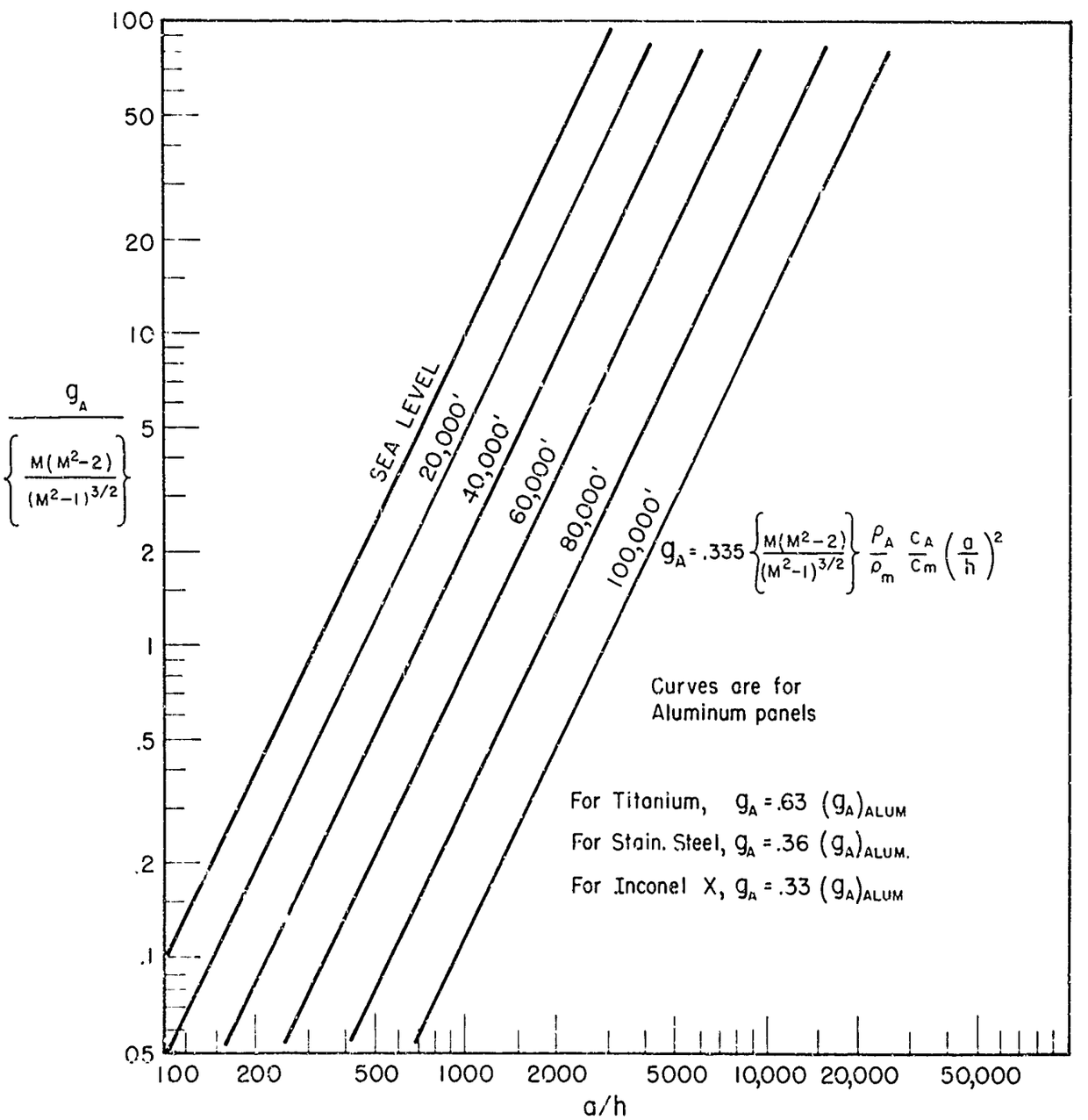

FIG. 2 MAGNITUDE OF AERODYNAMIC DAMPING

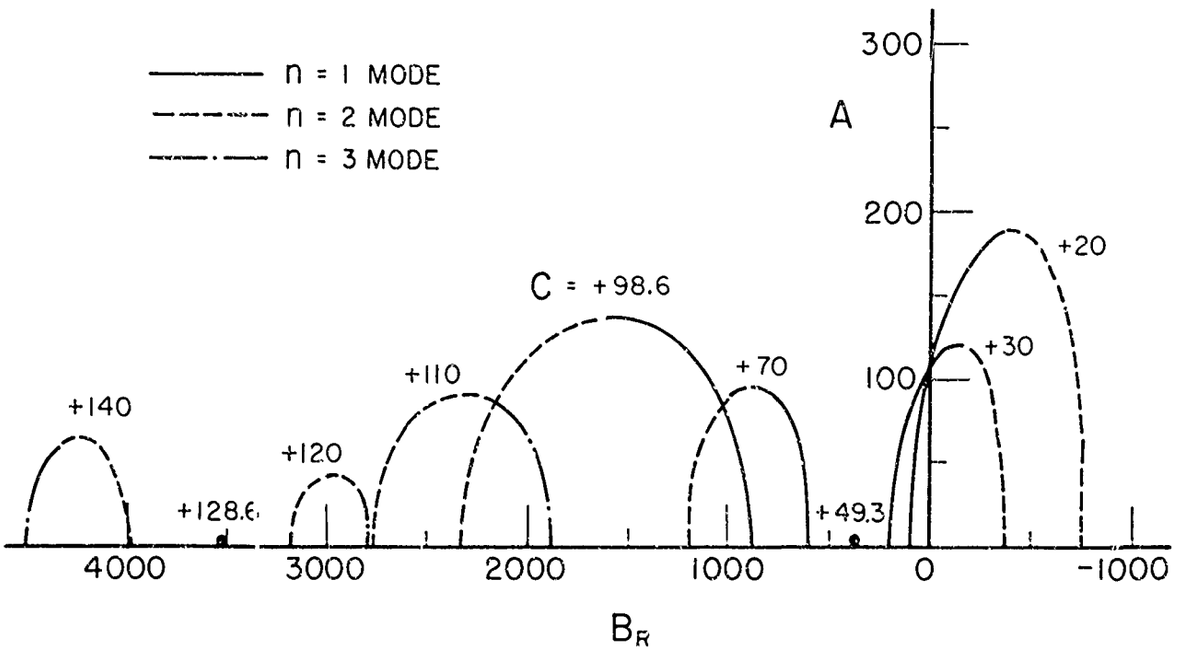

C	B_R FOR A = 0			
	n = 1	n = 2	n = 3	n = 4
0	-97	-1560	-7870	-24,900
30	199	-373	-5210	-20,200
49.3	388	388	-3500	-17,100
70	593	1200	-1660	-13,800
98.6	874	2330	874	-9,320
110	987	2780	1880	-7,530
120	1090	3170	2770	-5,950
128.6	1170	3520	3520	-4,590
140	1280	3960	4550	-2,790

FIG. 3a REAL EIGENVALUES ($B_I = 0$ CASE)

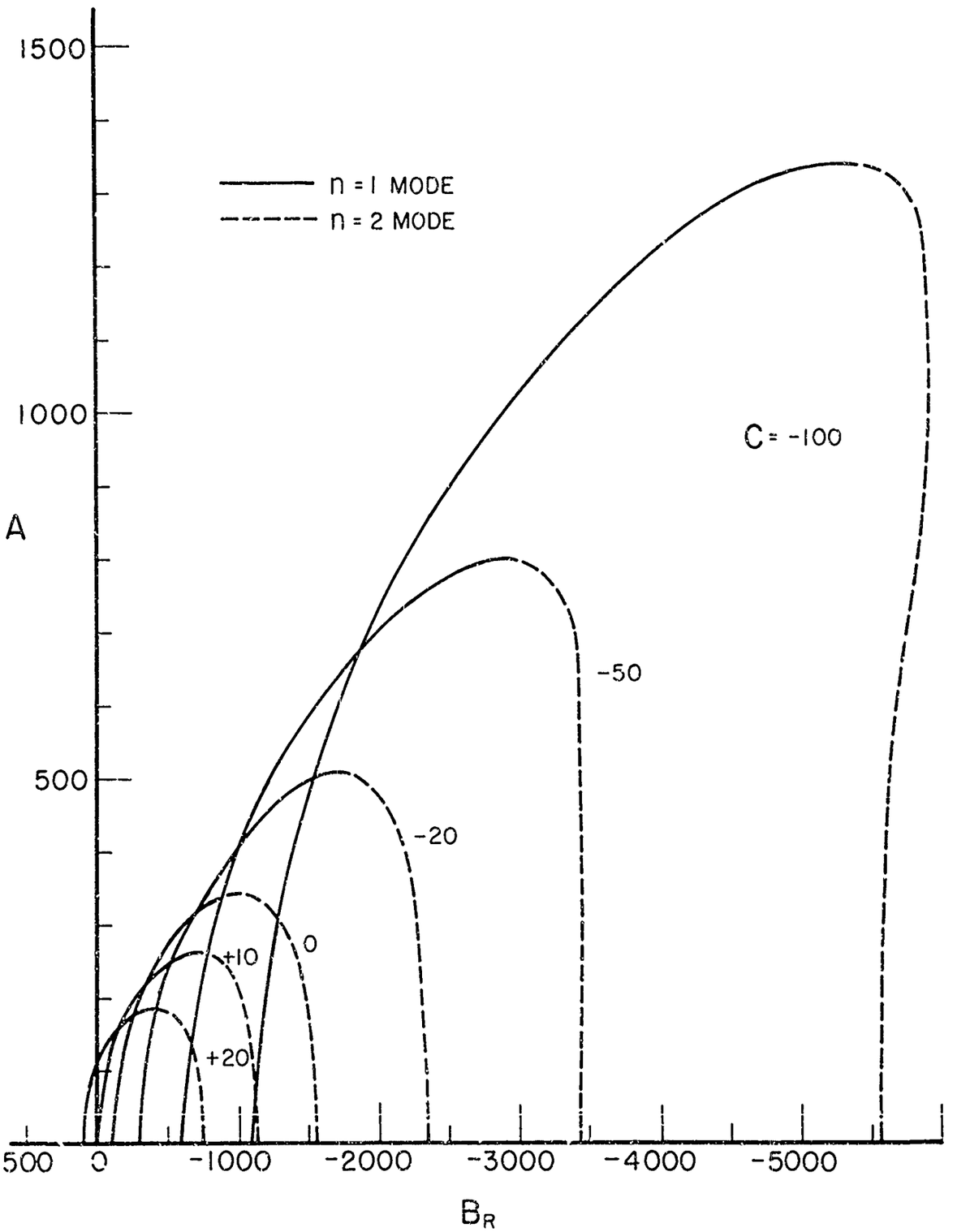

FIG. 3b REAL EIGENVALUES ($B_I = 0$ CASE)

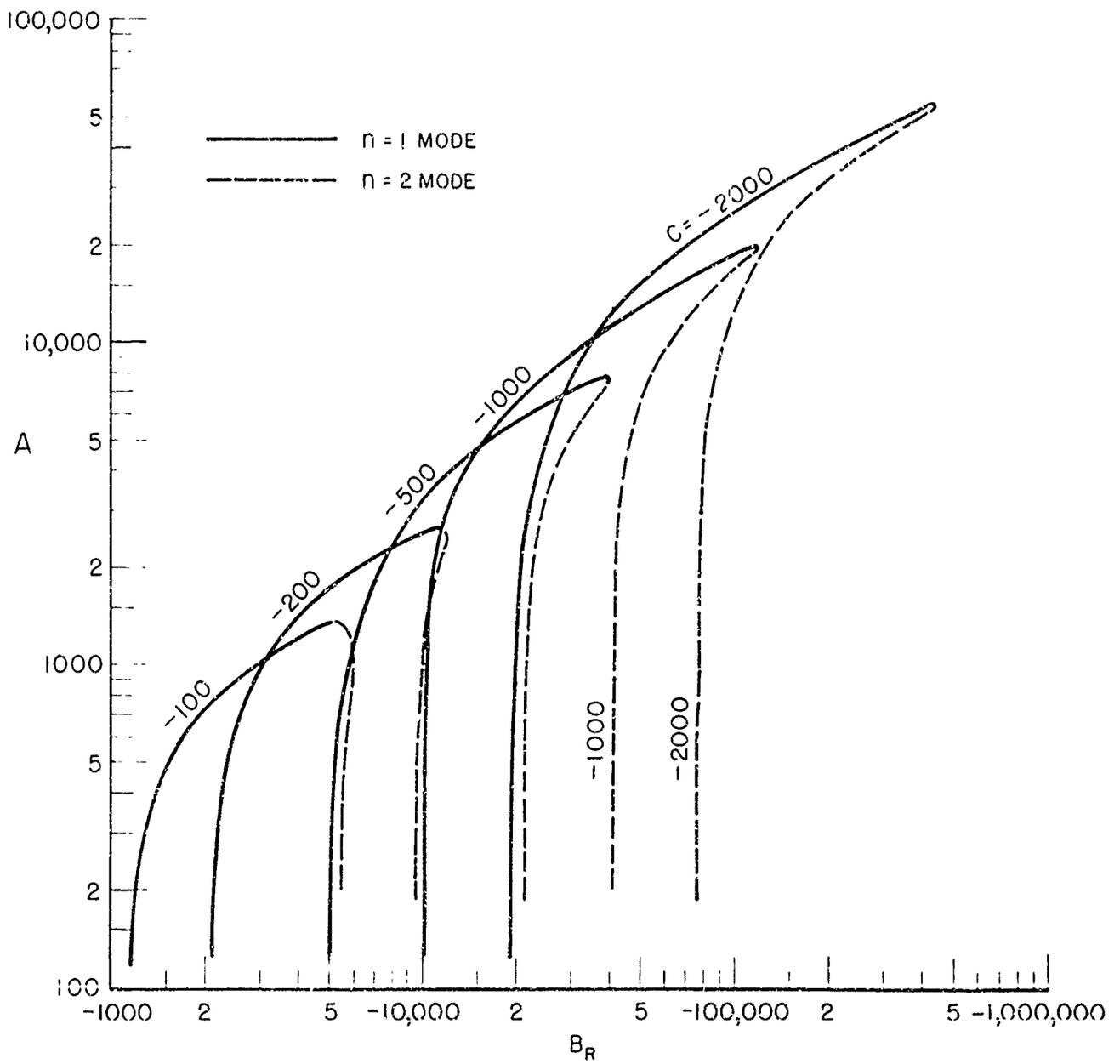

FIG. 3c REAL EIGENVALUES ($B_I = 0$ CASE)

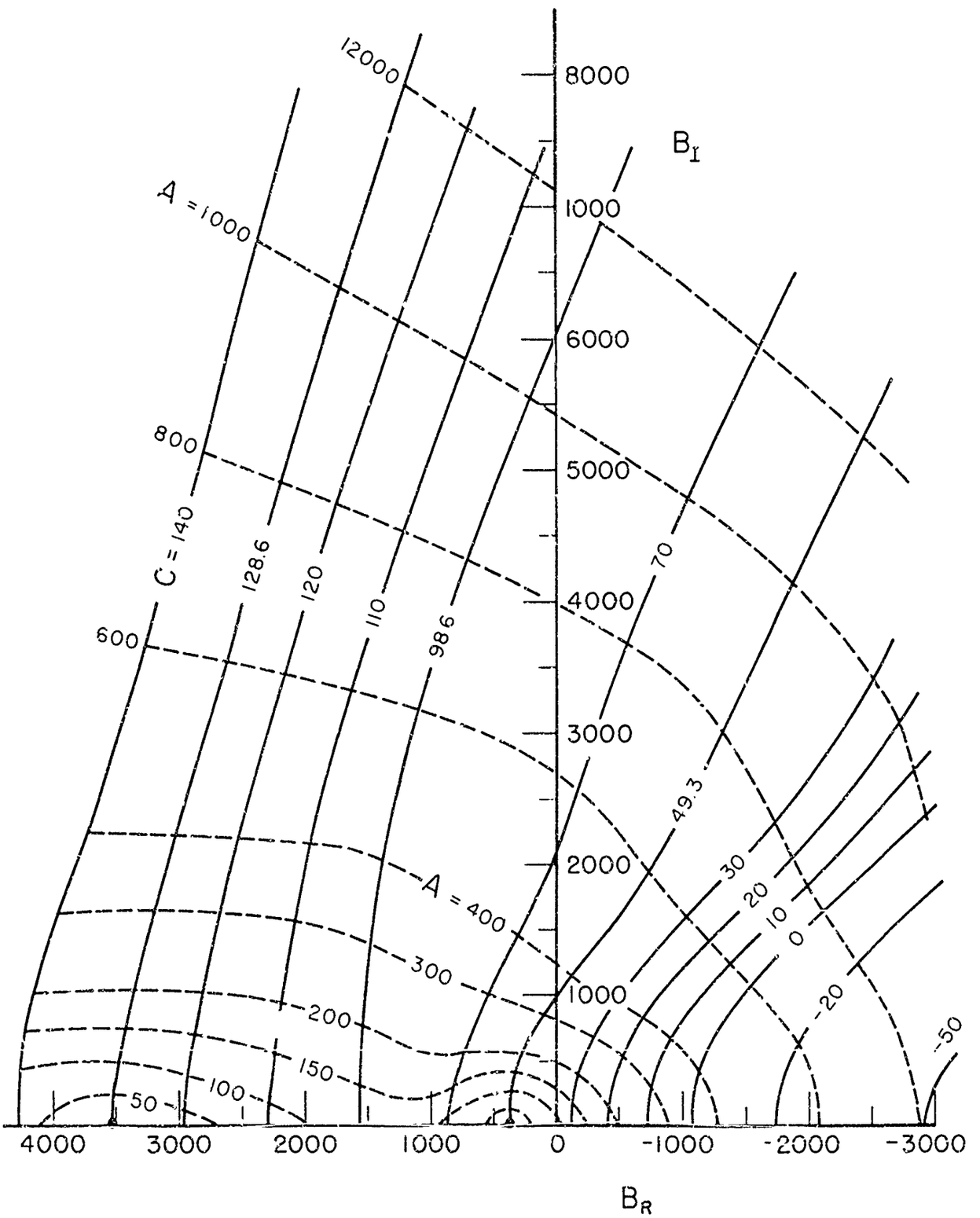

FIG. 4a COMPLEX EIGENVALUES

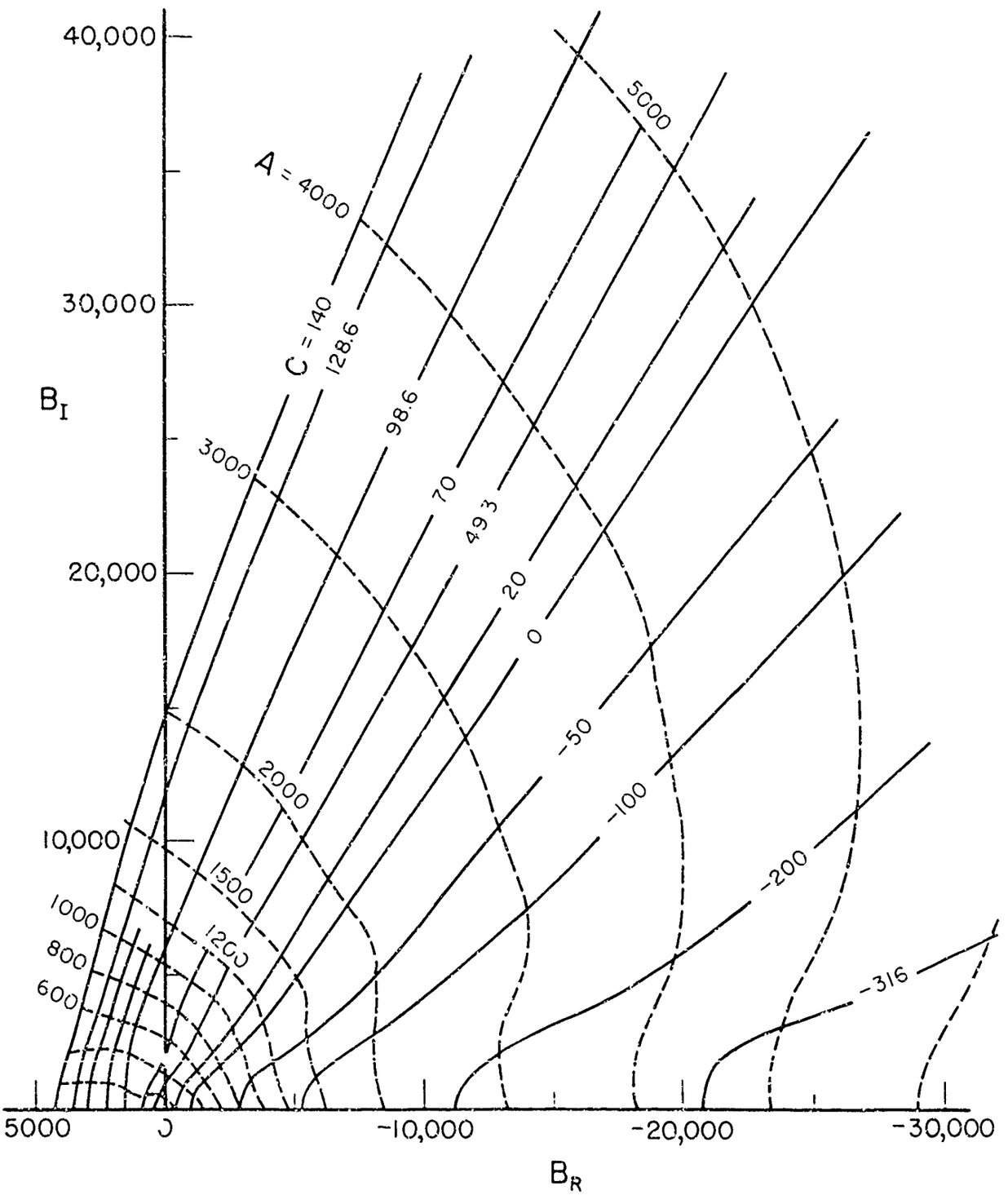

FIG 4b COMPLEX EIGENVALUES

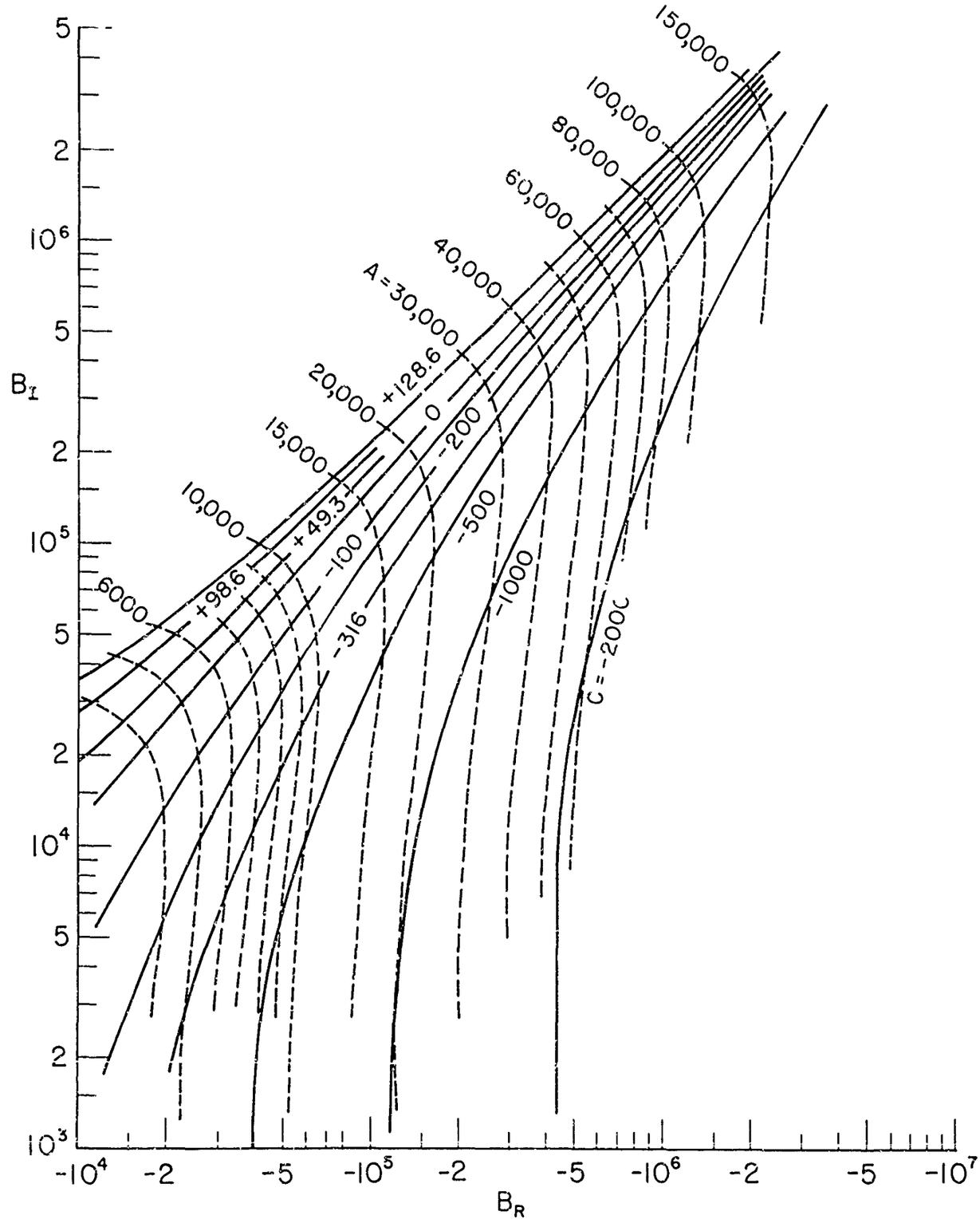

FIG. 4c COMPLEX EIGENVALUES

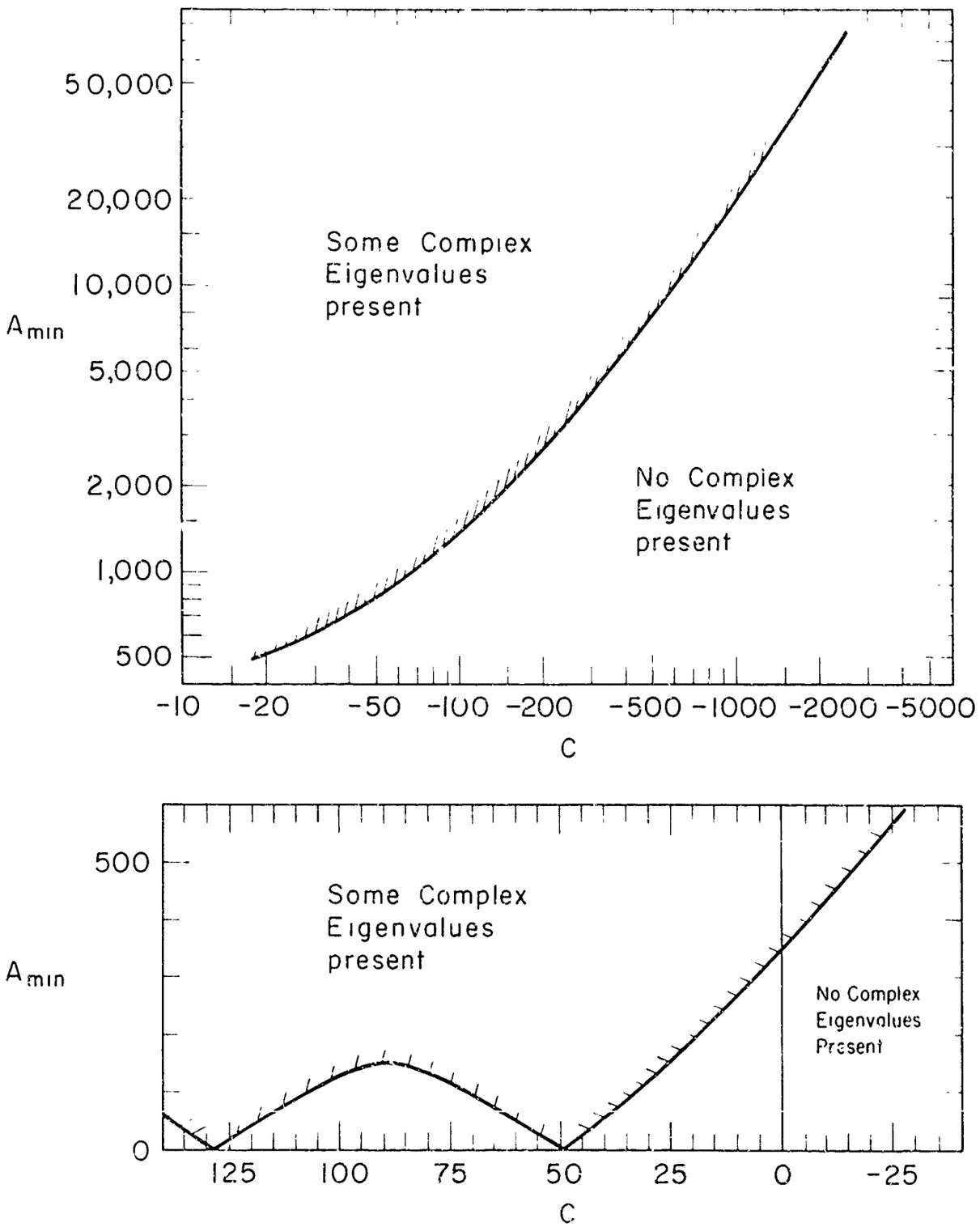

FIG. 5 MINIMUM VALUE OF A FOR FLUTTER

$$W(\xi,\eta,\tau) = \bar{W}(\xi)\left[\sin m\pi\eta\right]e^{(\bar{\alpha}+i\bar{\omega})\tau}$$

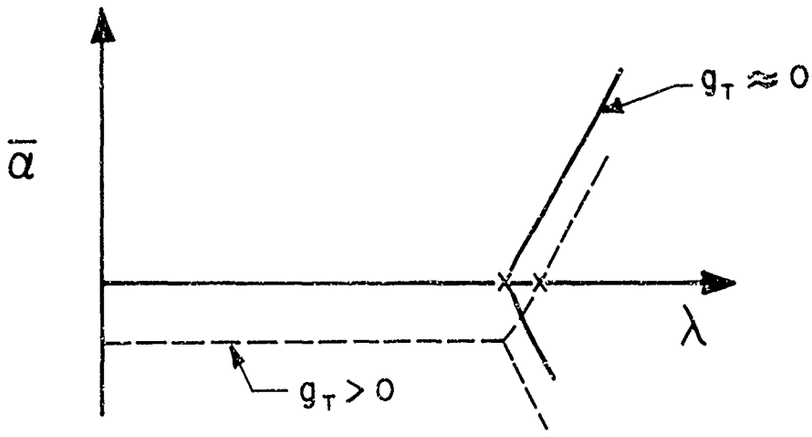

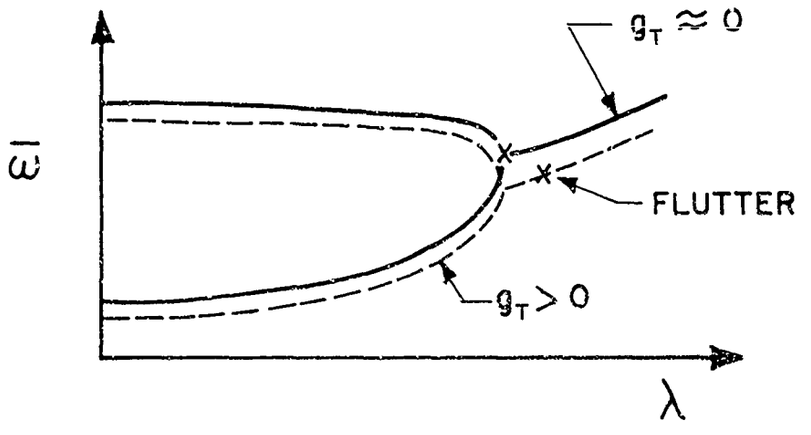

"Frequency Coalescence Flutter"

FIG. 6 TYPICAL PLOTS OF PANEL BEHAVIOR

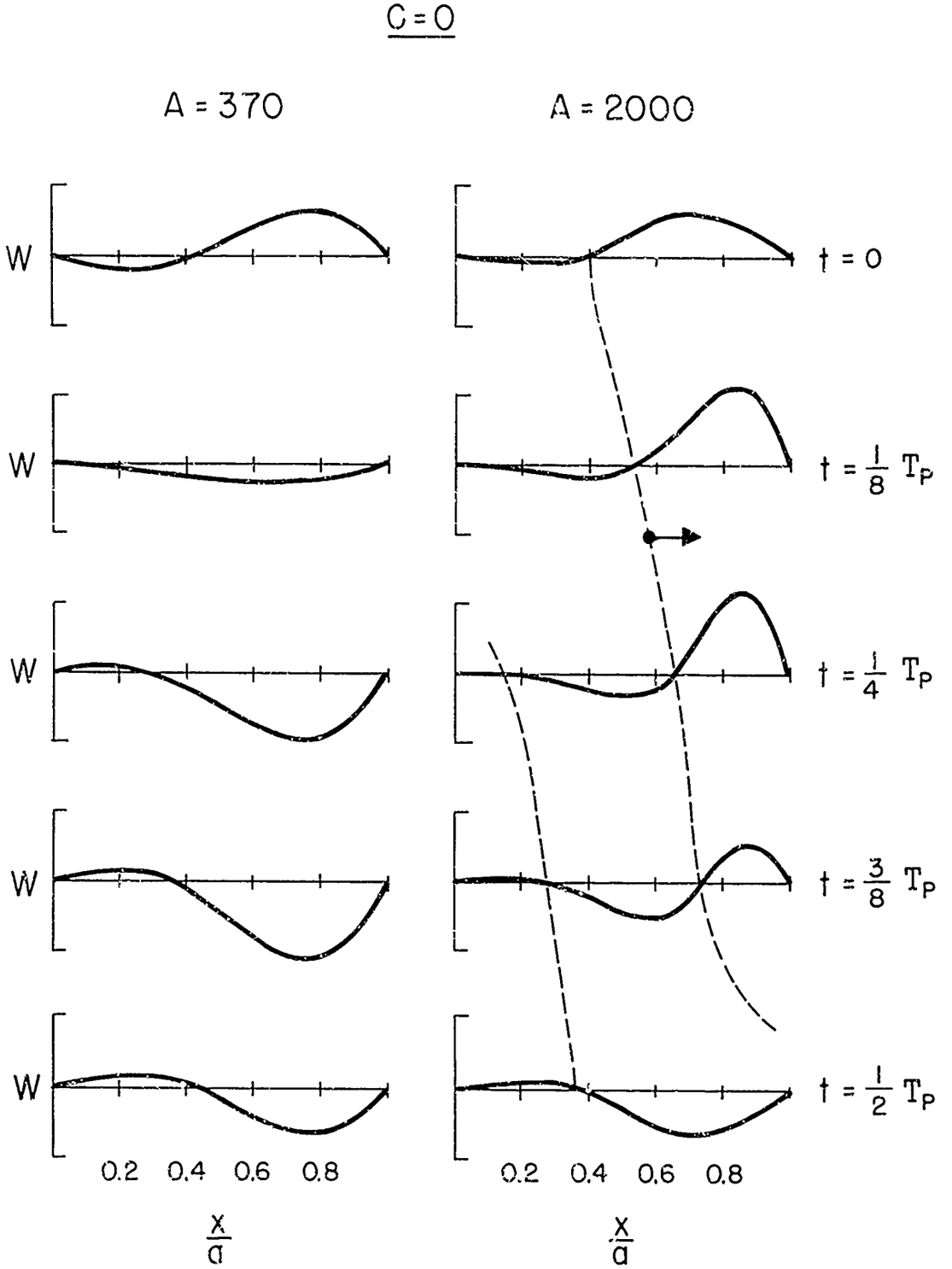

FIG. 7a, b MODE SHAPES

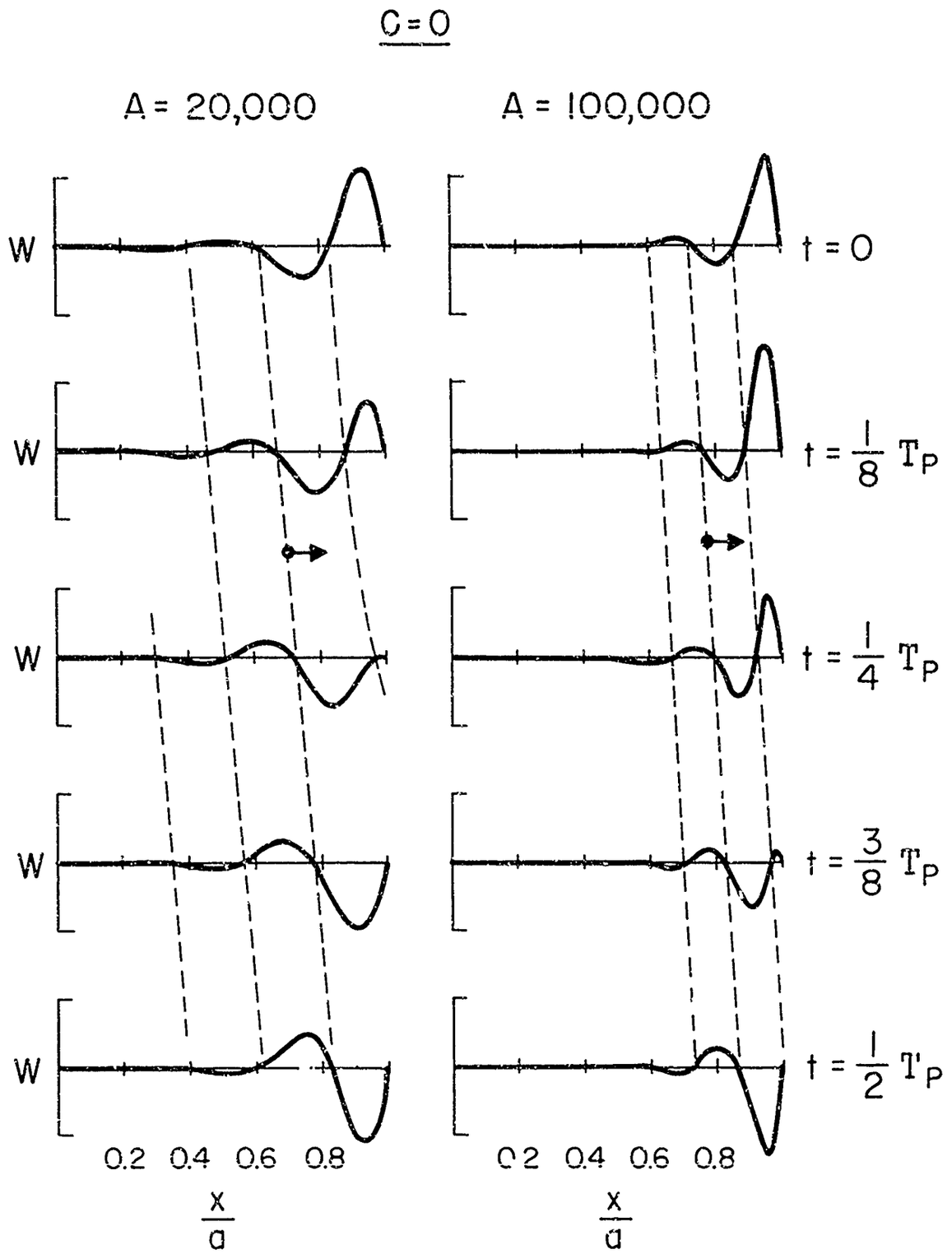

FIG. 7c, d MODE SHAPES

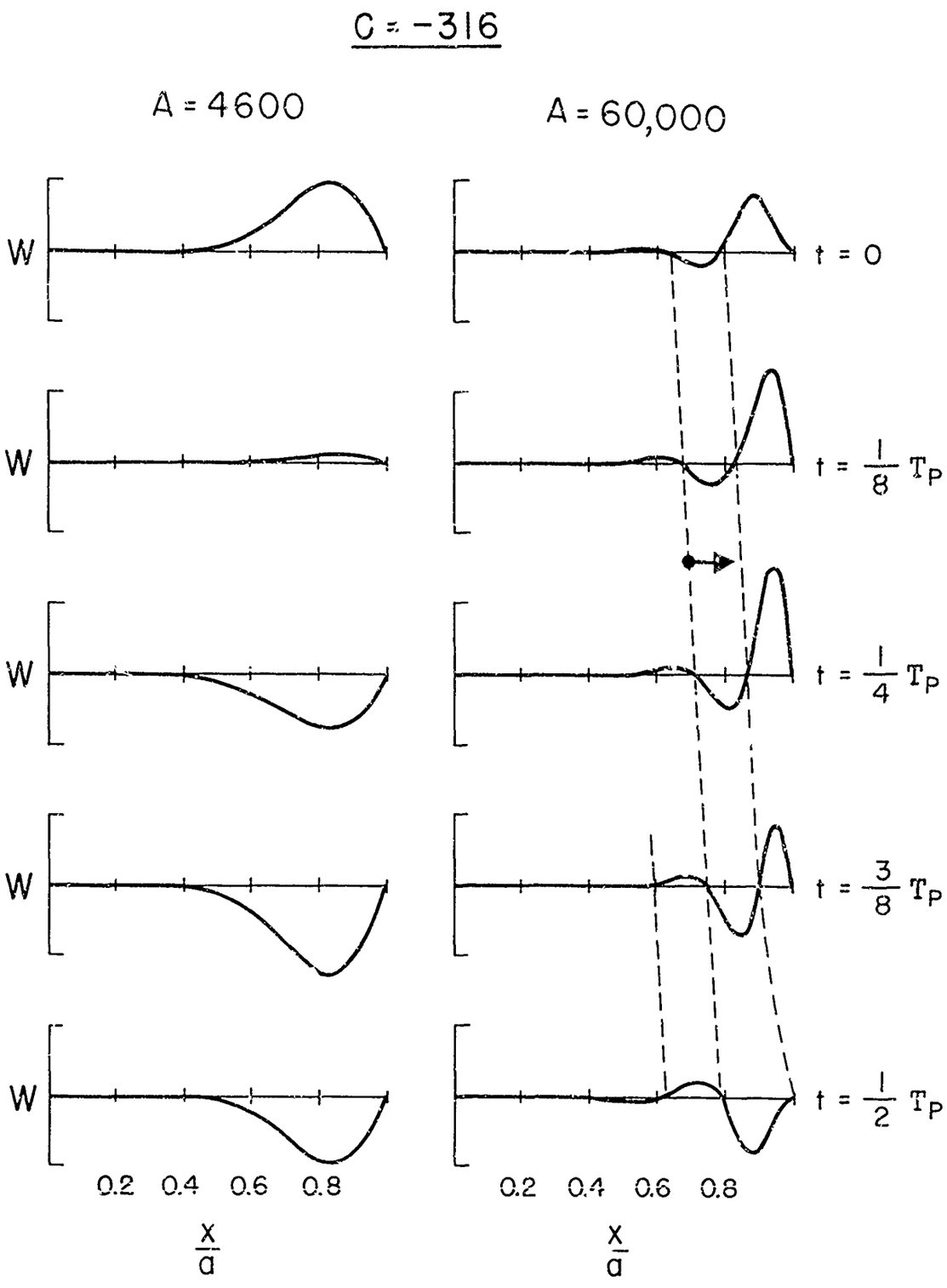

FIG. 7e, f MODE SHAPES

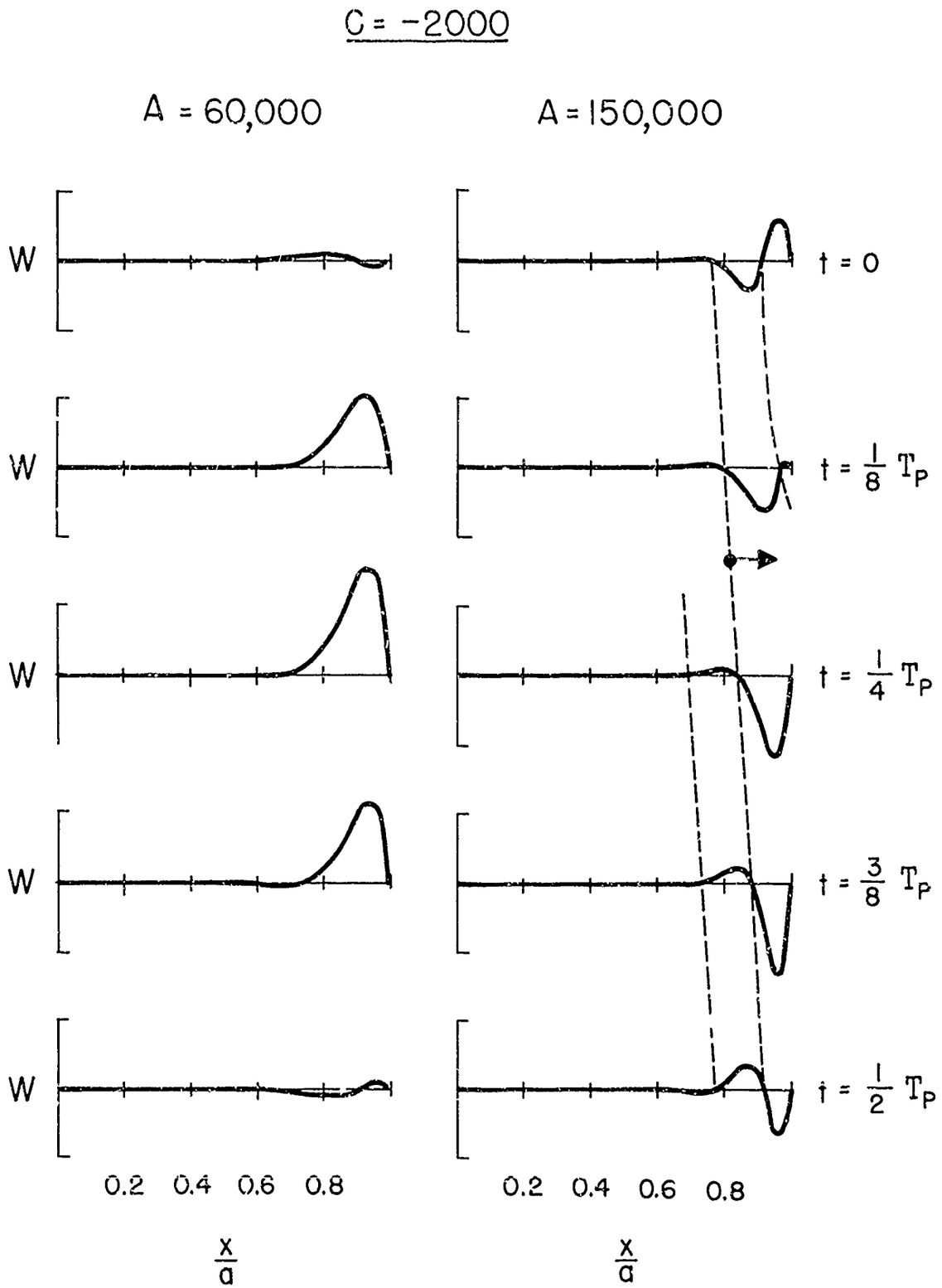

FIG. 7g, h MODE SHAPES

C = 49.3

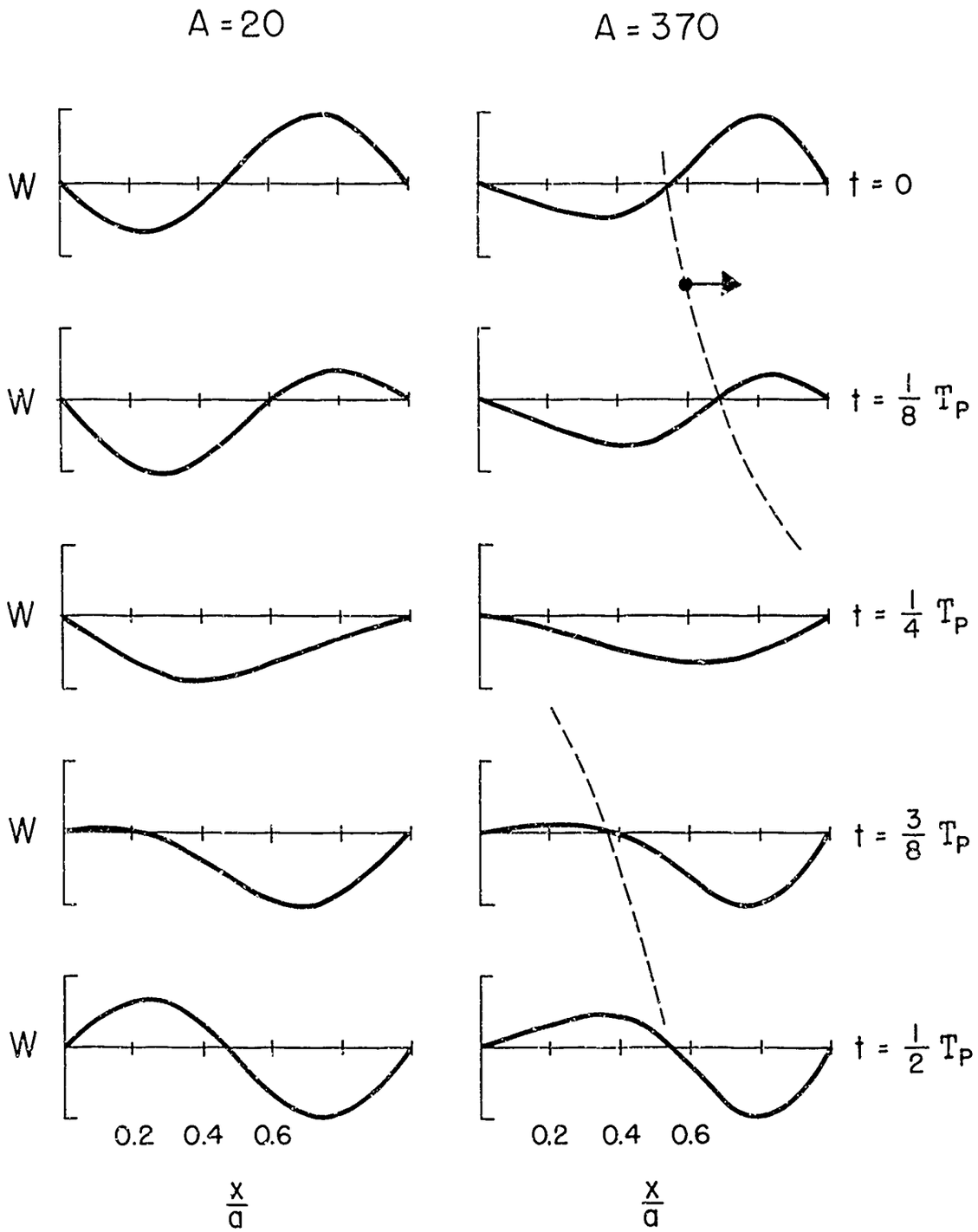

FIG. 7i, j MODE SHAPES

C = 98.6

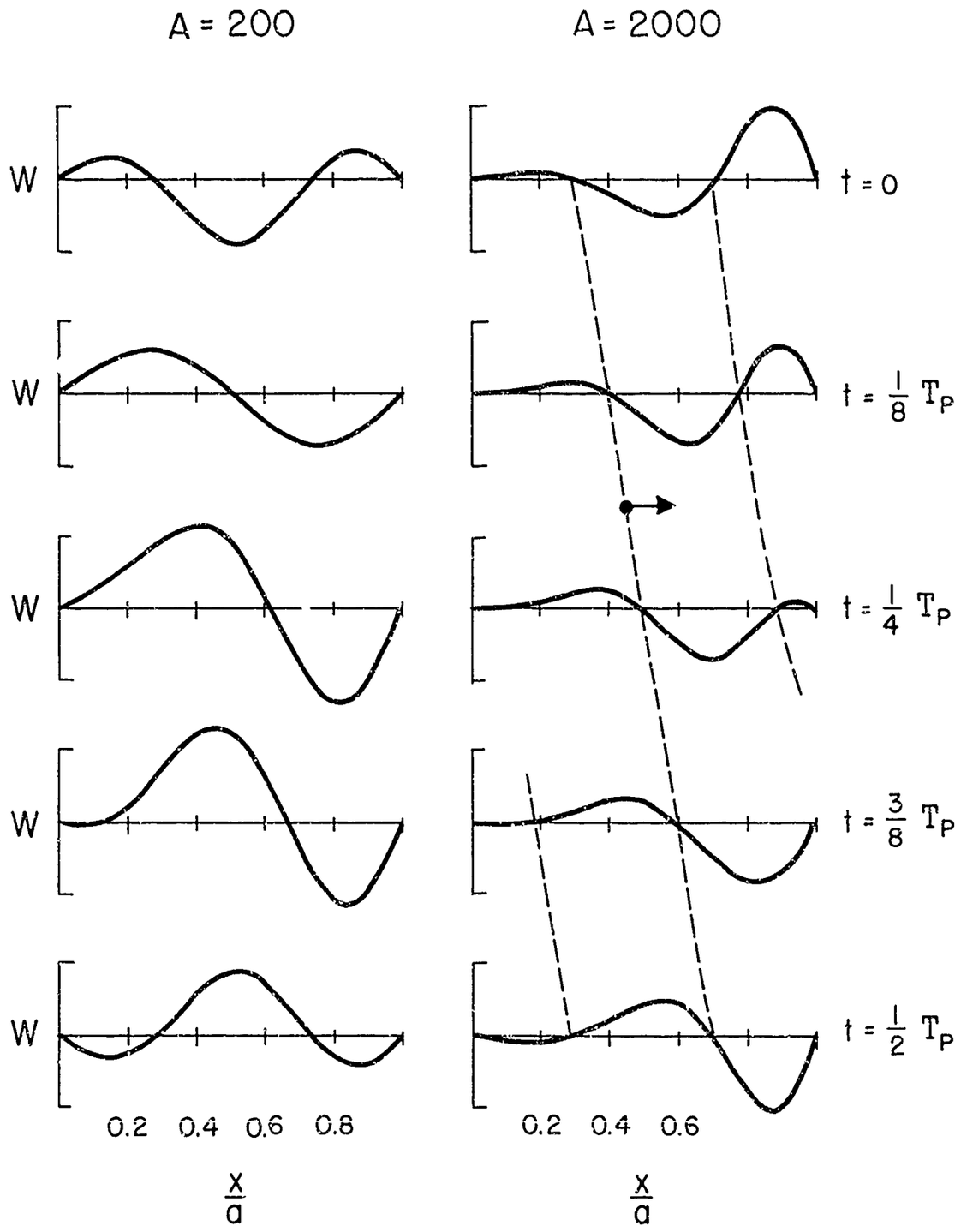

FIG. 7k, ℓ MODE SHAPES

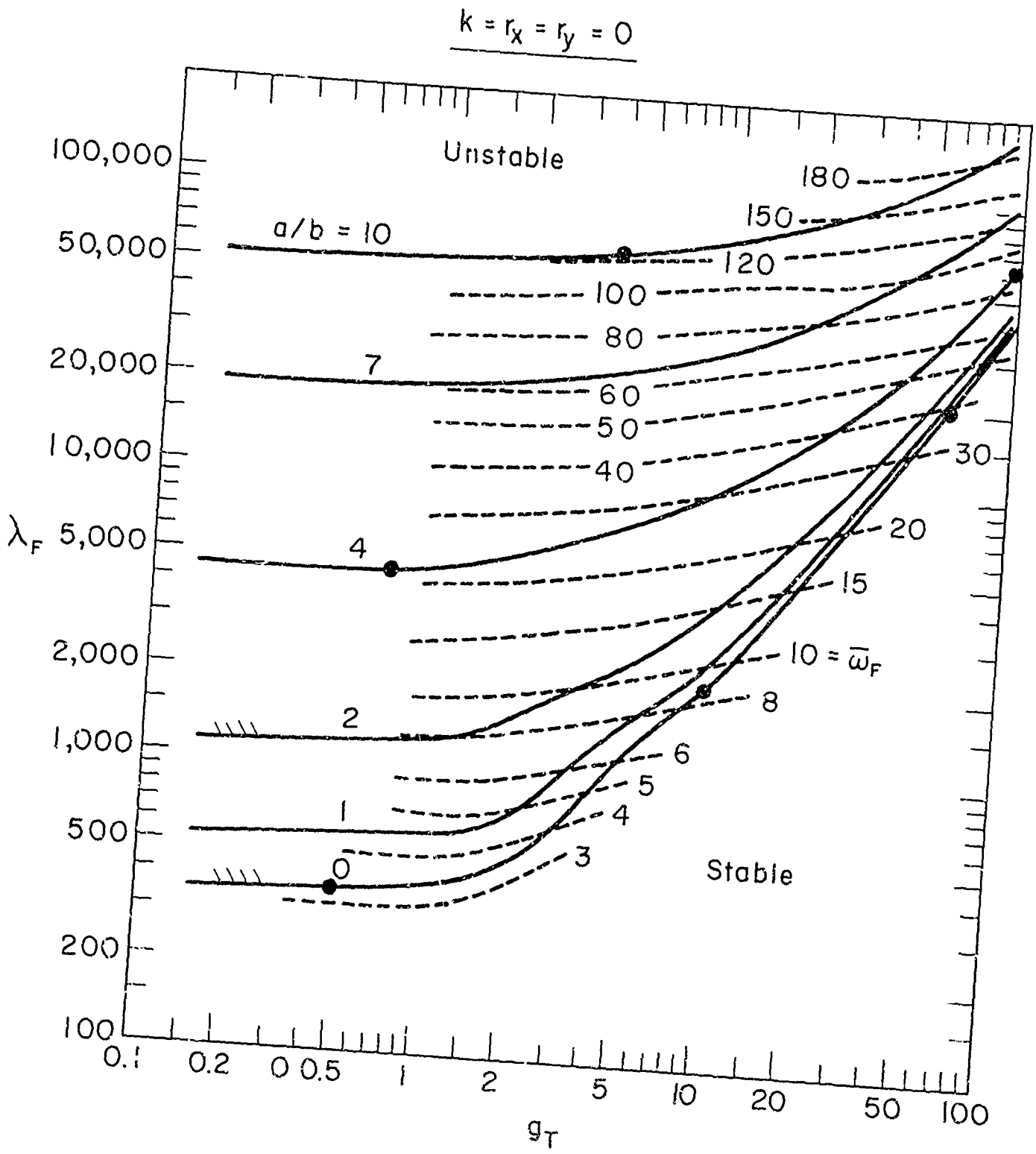

FIG. 8 PURE ASPECT RATIO EFFECT

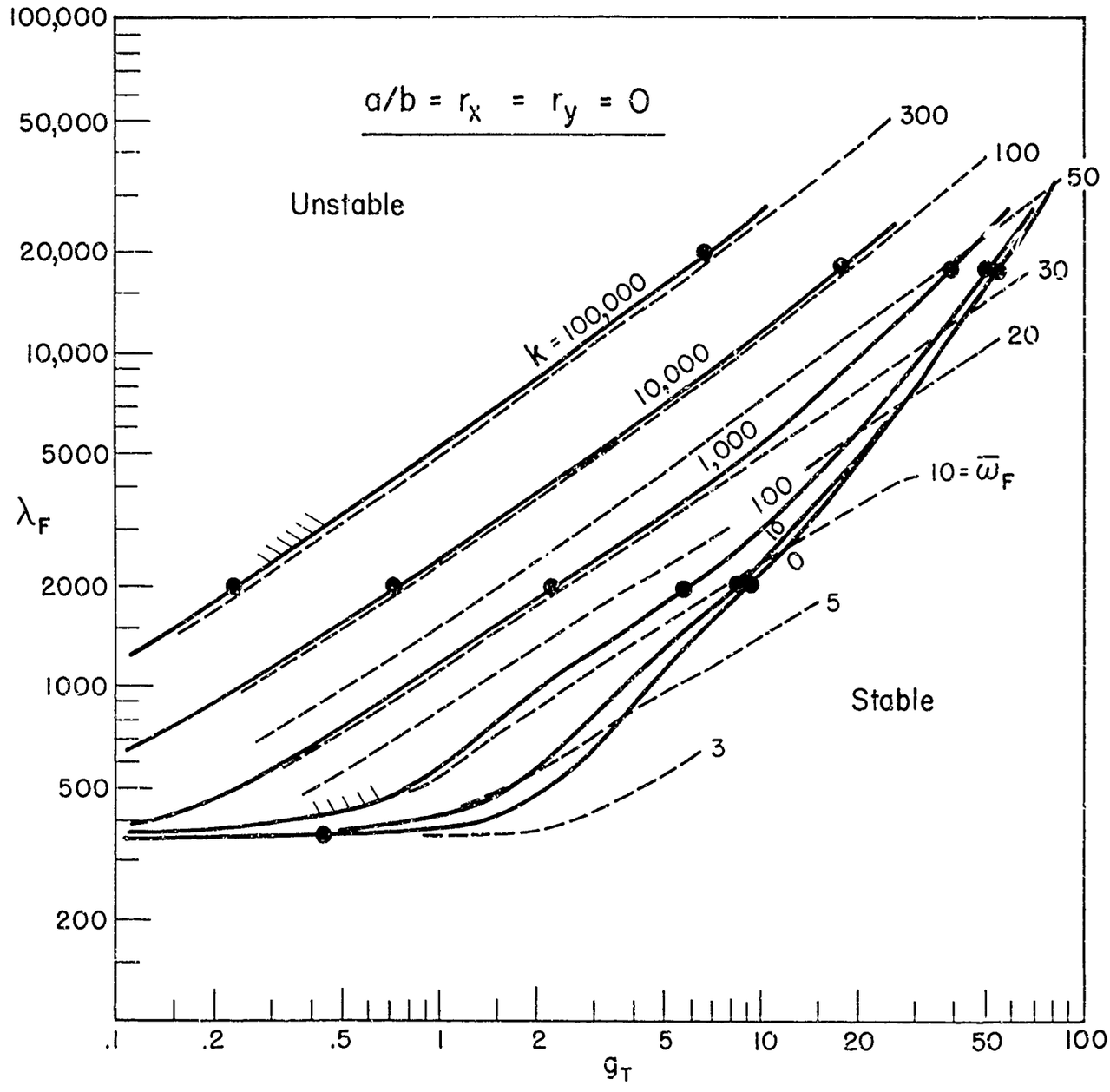

FIG. 9 PURE SPRING EFFECT

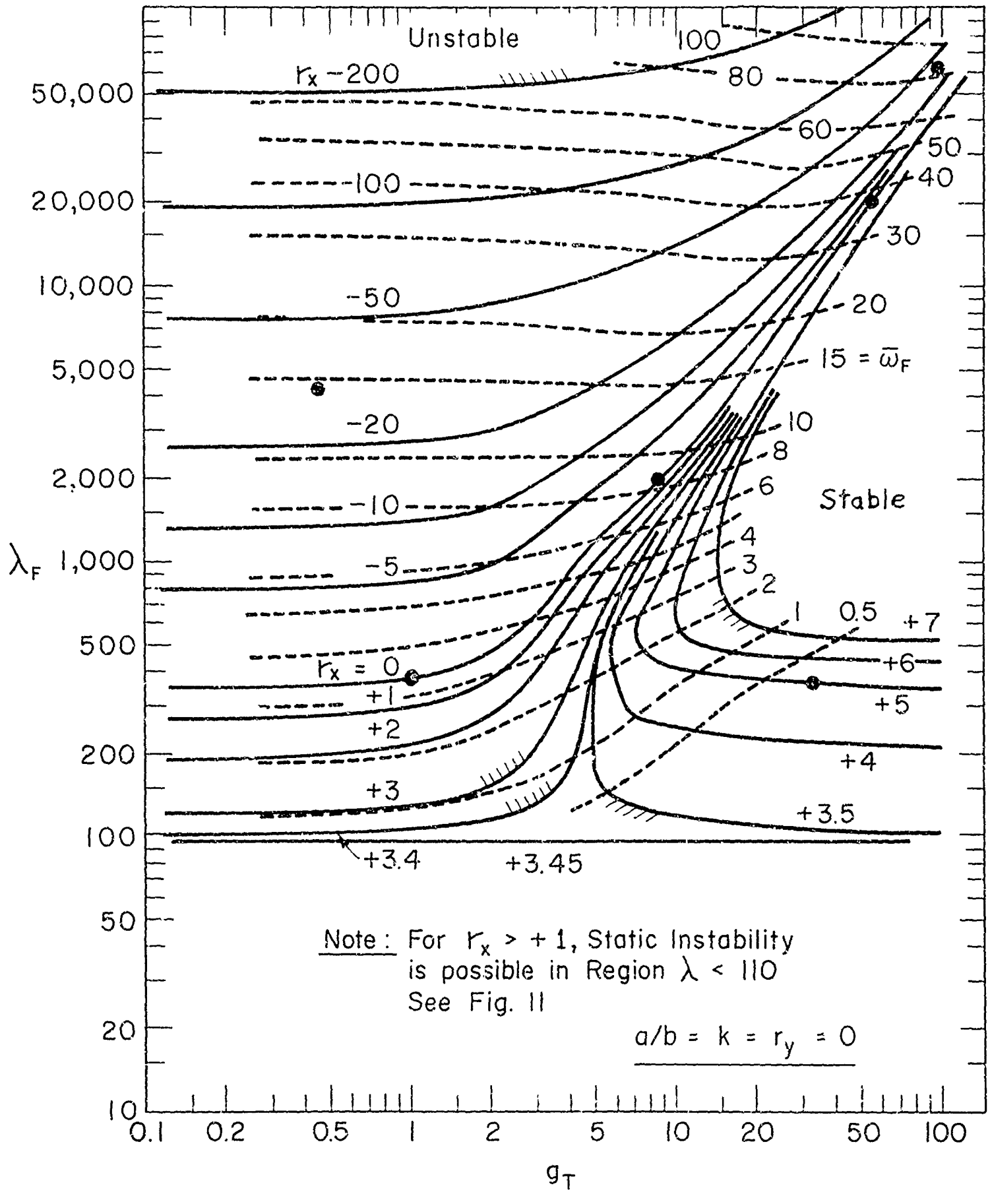

FIG. 10 PURE LONGIT. COMPRESSION EFFECT

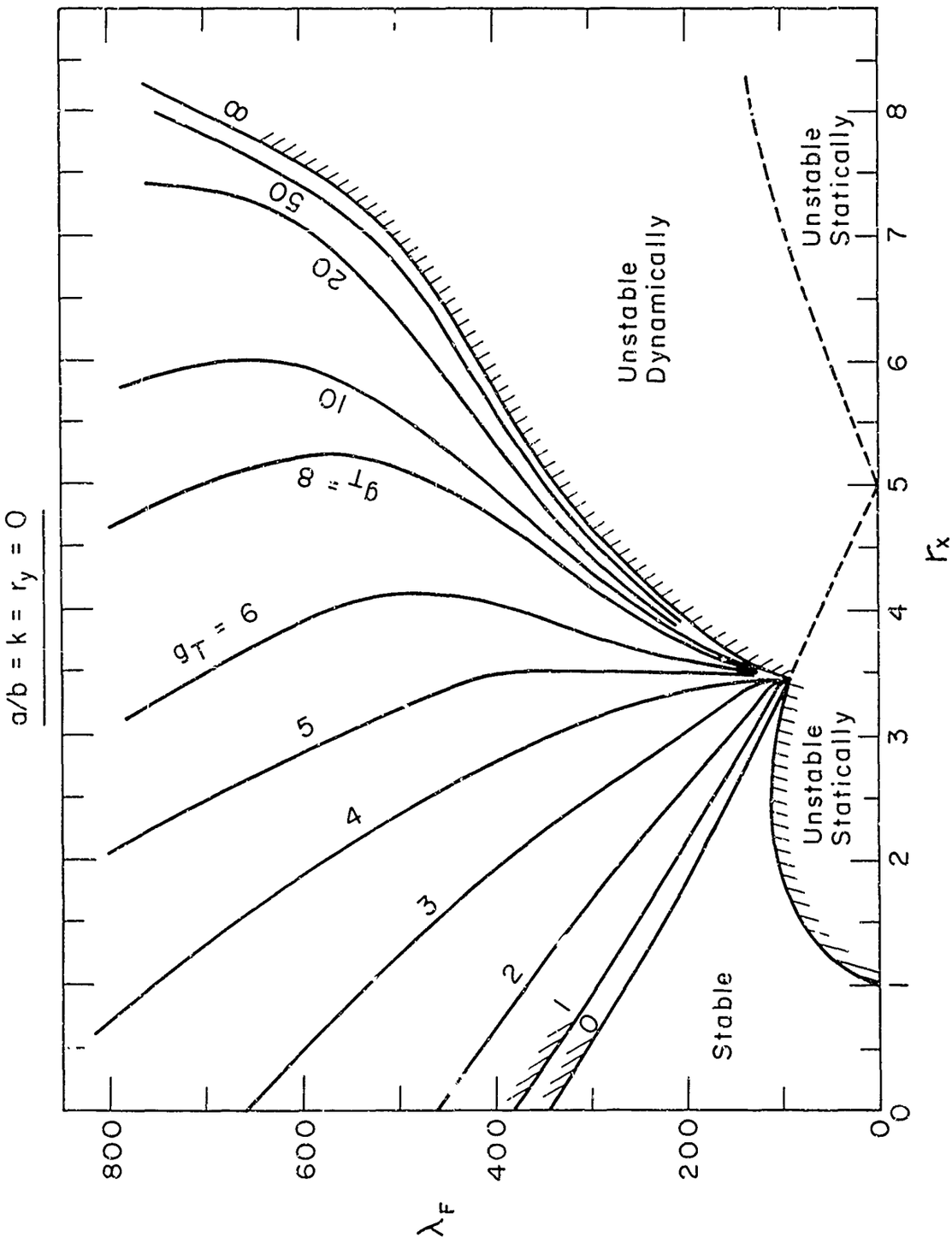

FIG. 11 PURE LONGIT. COMPRESSION EFFECT

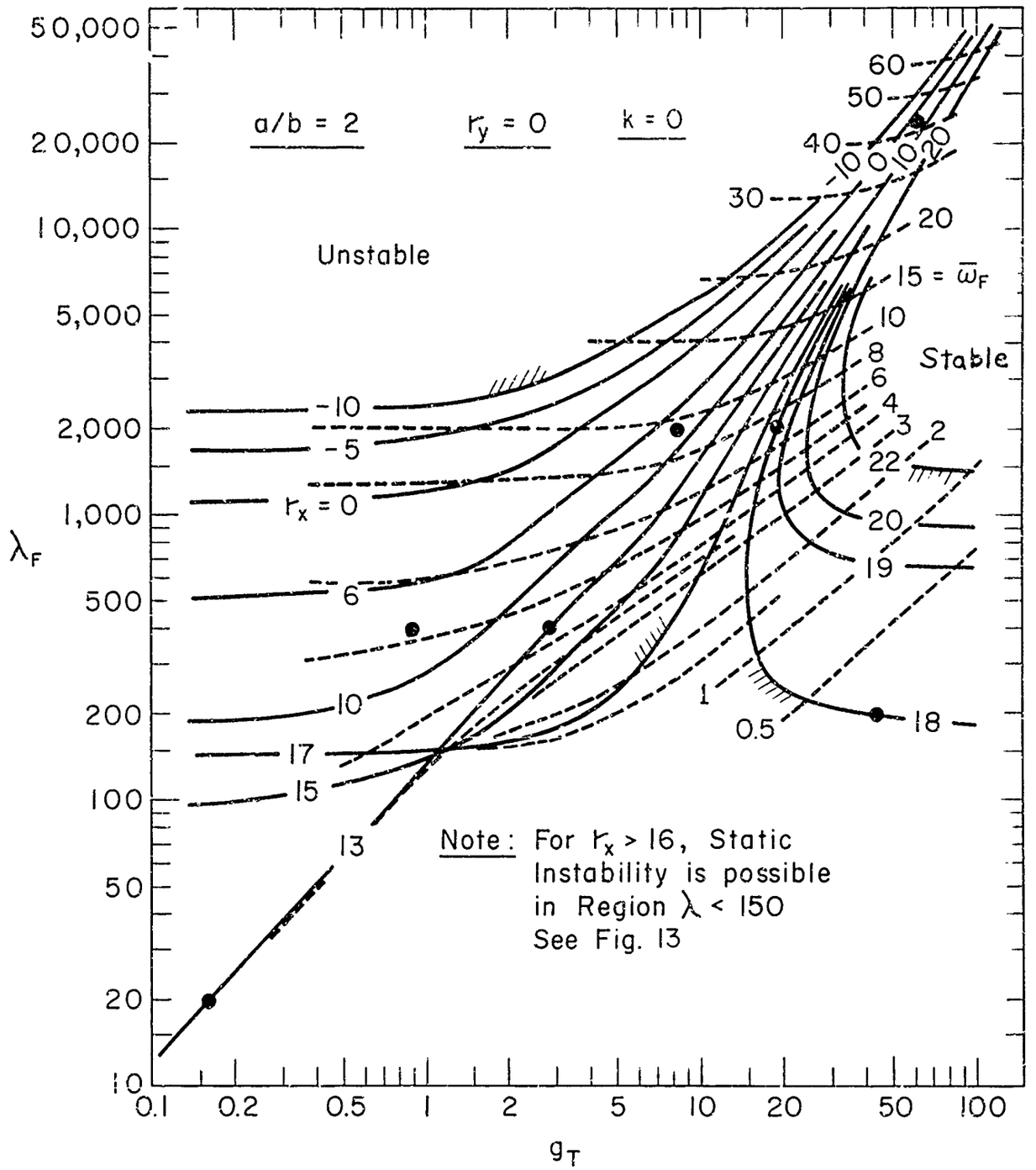

FIG. 12 COMBINED COMPRESSION AND ASPECT RATIO (a)

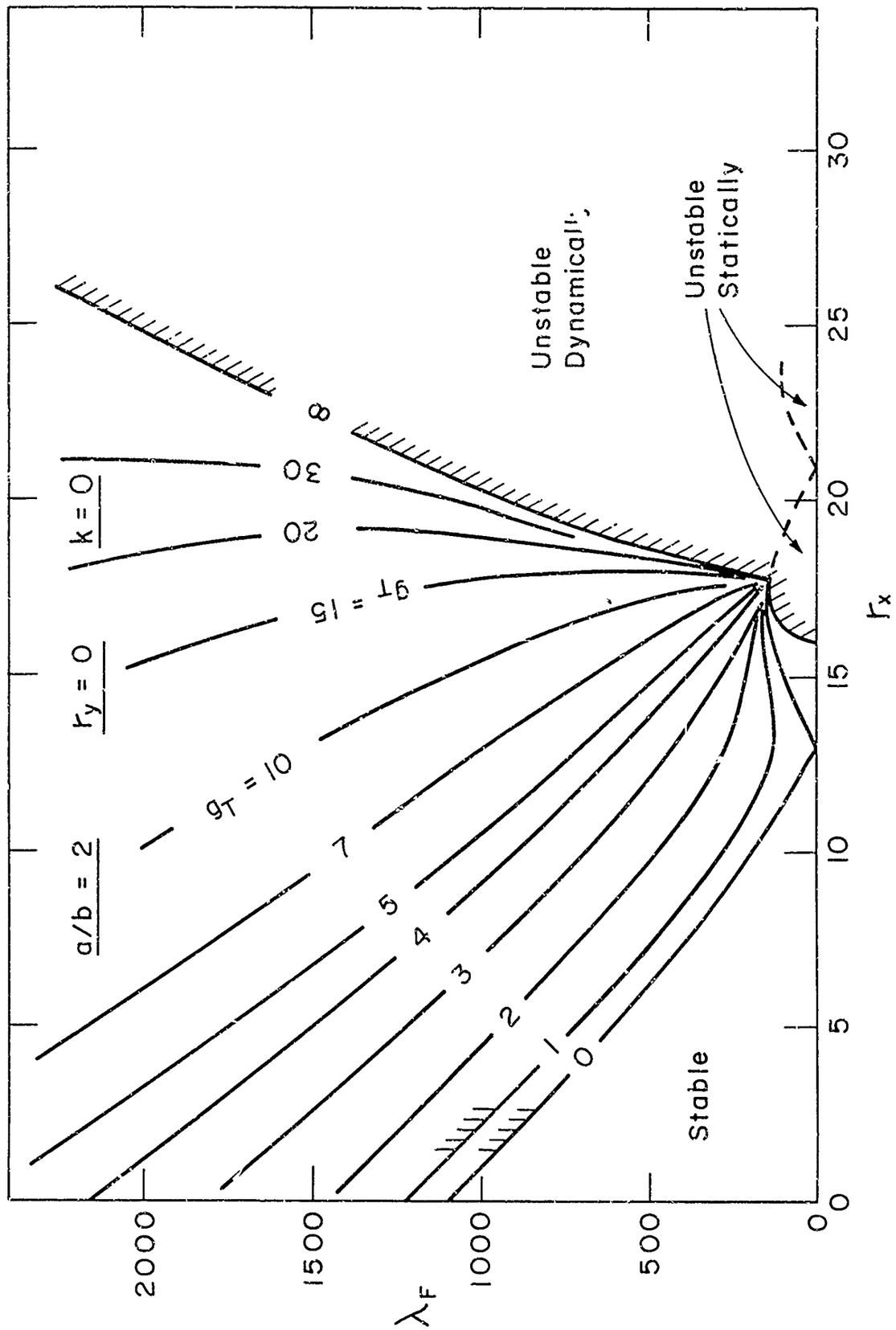

FIG. 13 COMBINED COMPRESSION AND ASPECT RATIO (a)

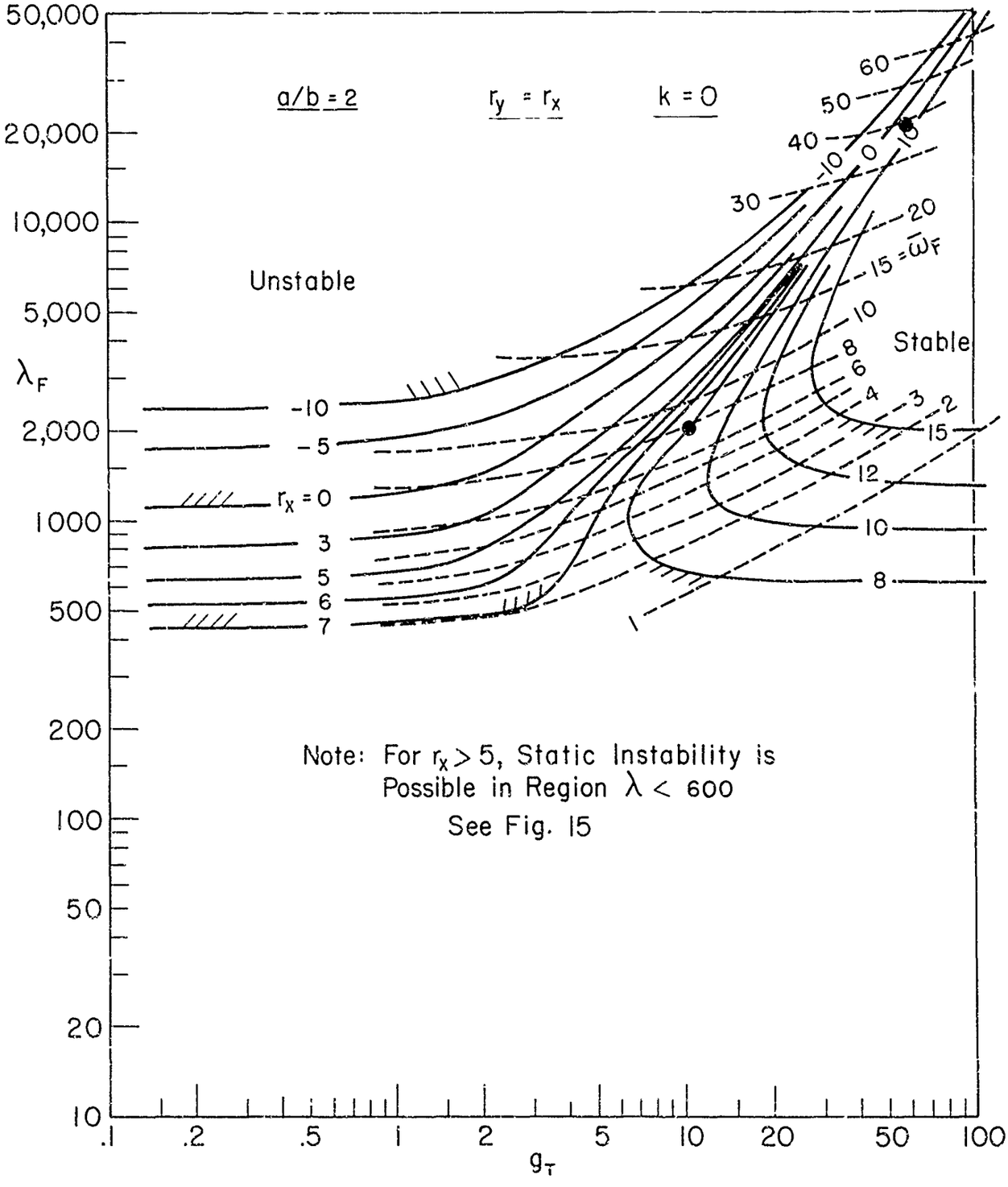

FIG. 14 COMBINED COMPRESSION AND ASPECT RATIO (b)

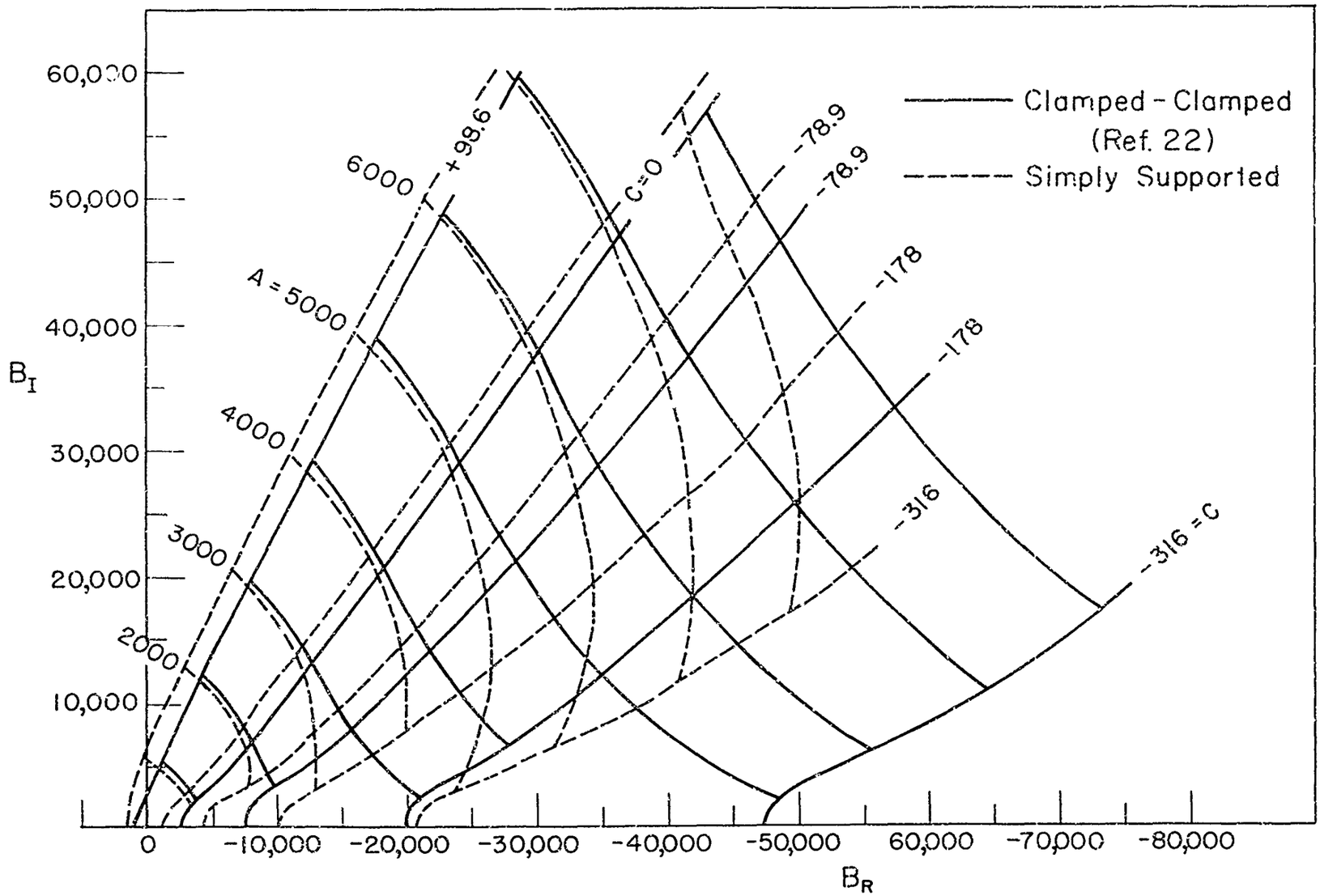

FIG. 16 COMPLEX EIGENVALUES FOR OTHER BOUNDARY CONDITIONS

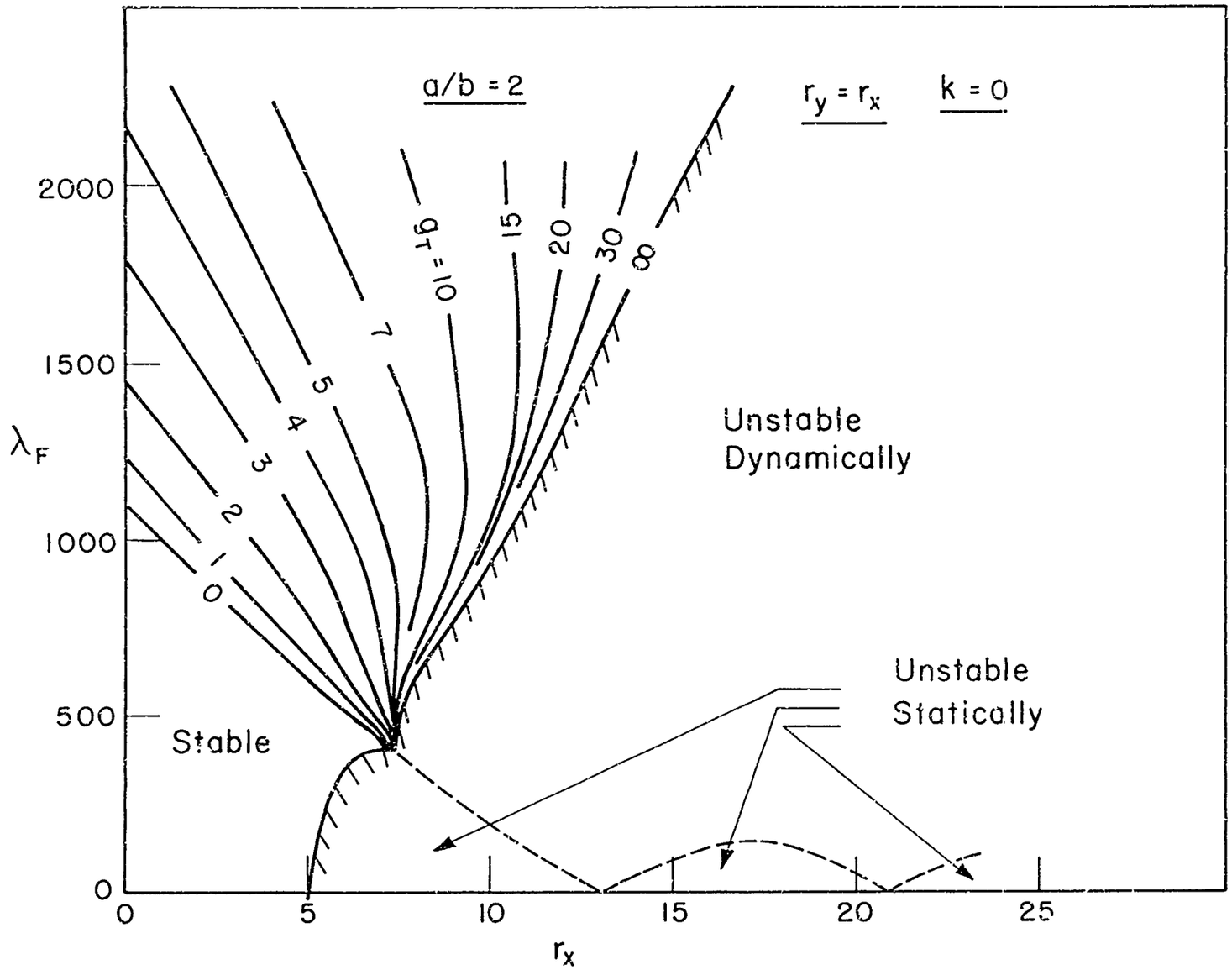

FIG. 15 COMBINED COMPRESSION AND ASPECT RATIO (b)

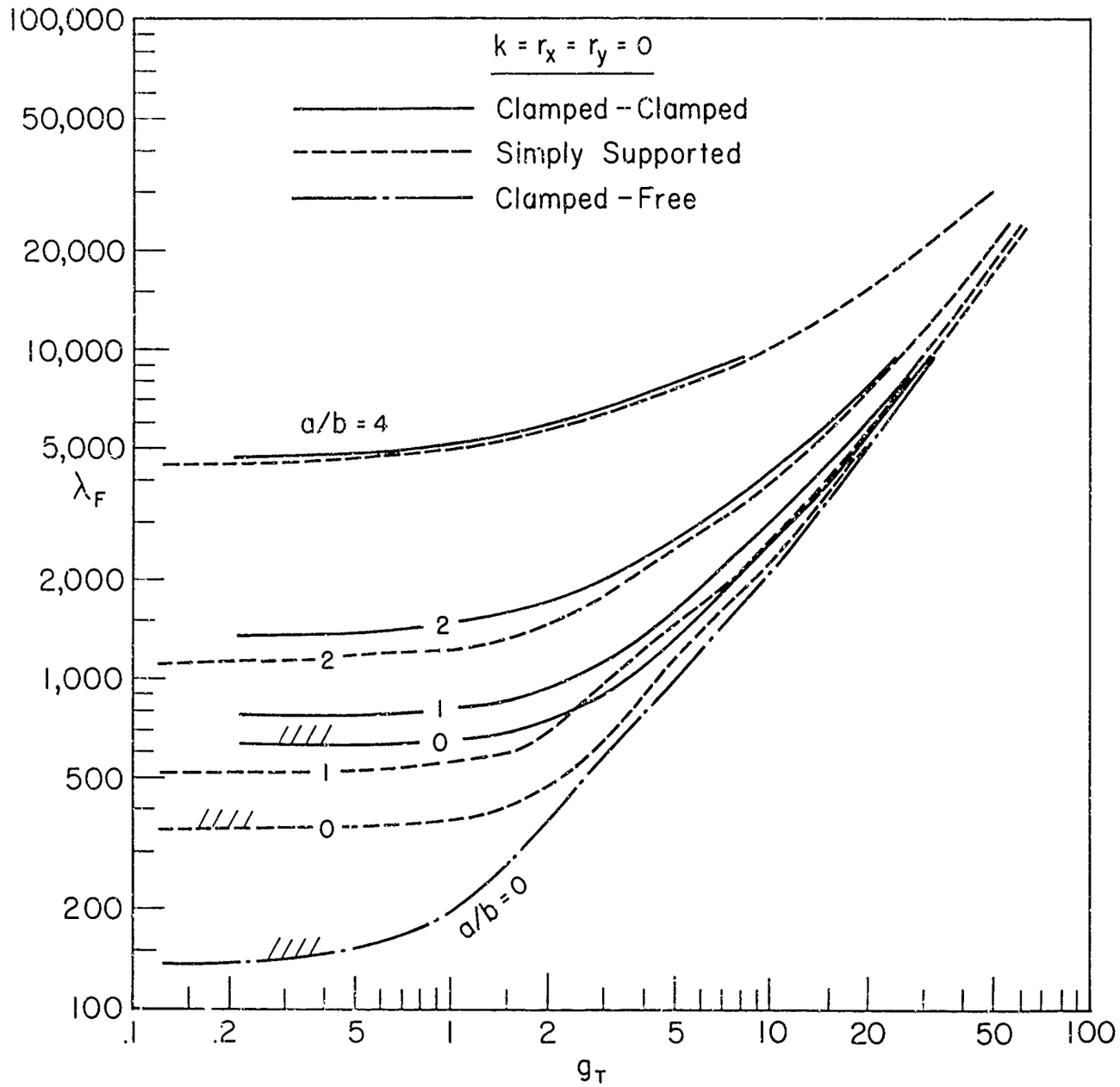

FIG. 17 BOUNDARY SUPPORT EFFECT

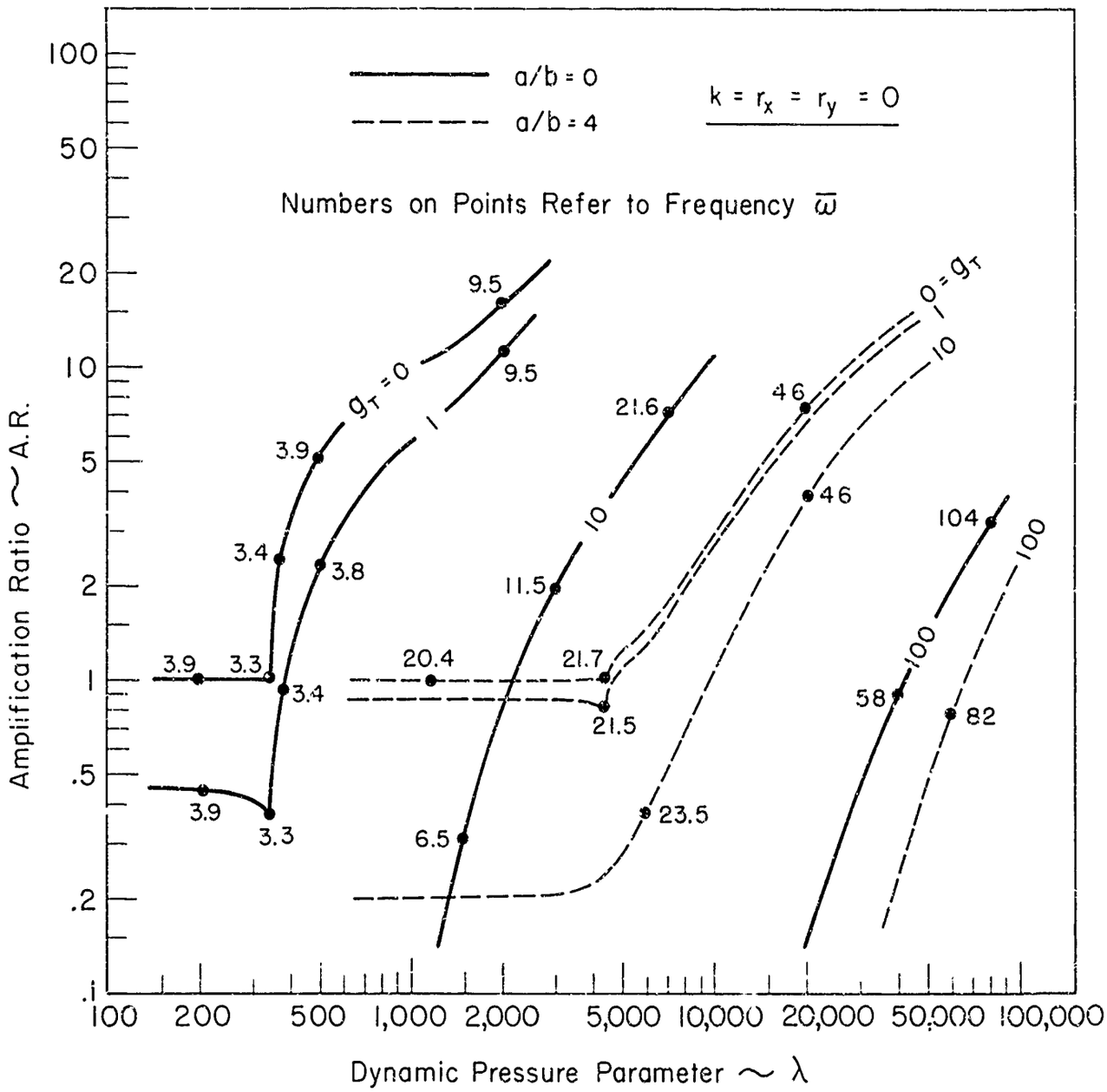

FIG. 18 AMPLIFICATION RATIO VS. DYNAMIC PRESSURE PARAMETER

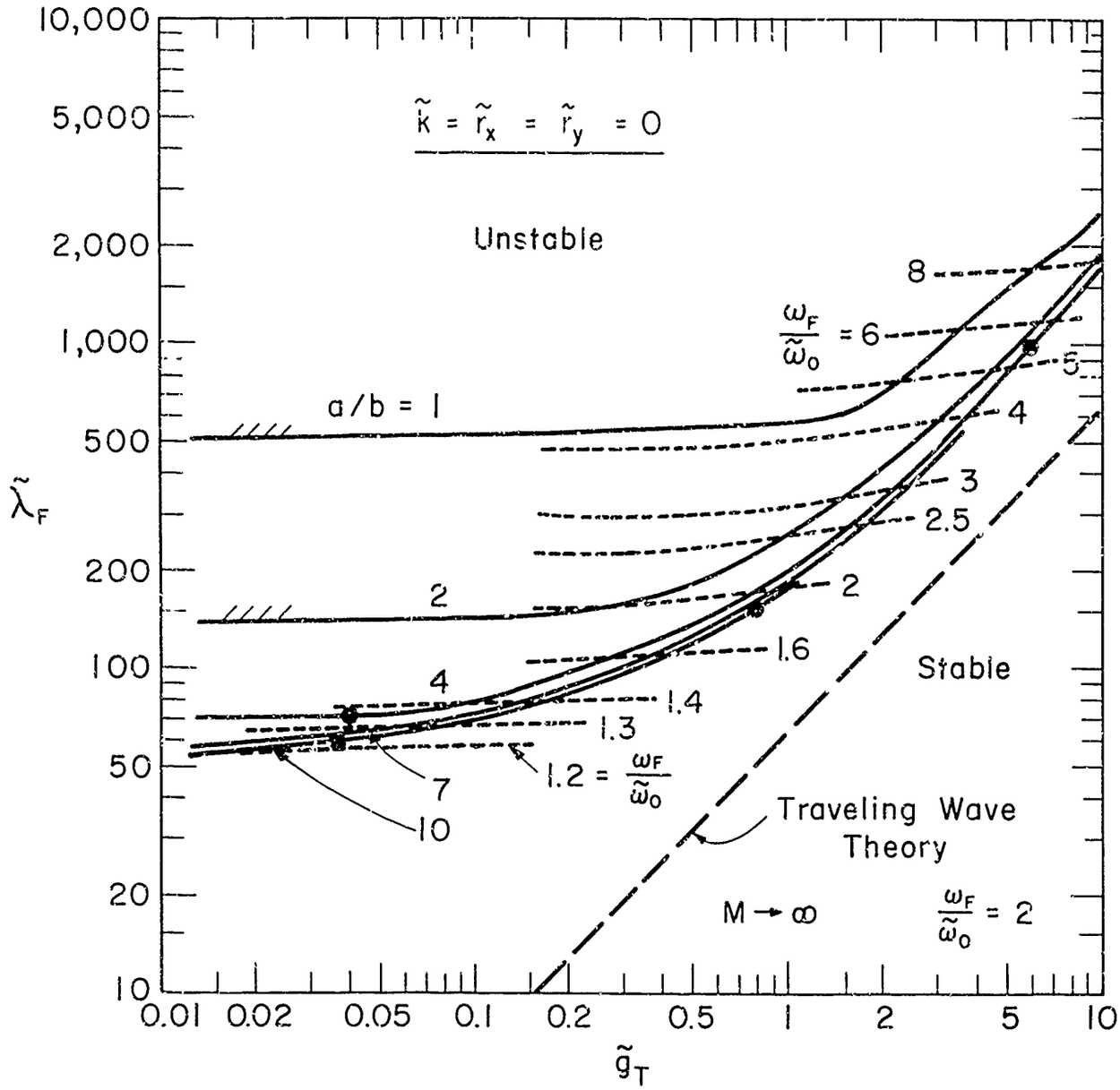

FIG. 19 COMPARISON OF TRAVELING WAVE AND FINITE PANEL ANALYSES

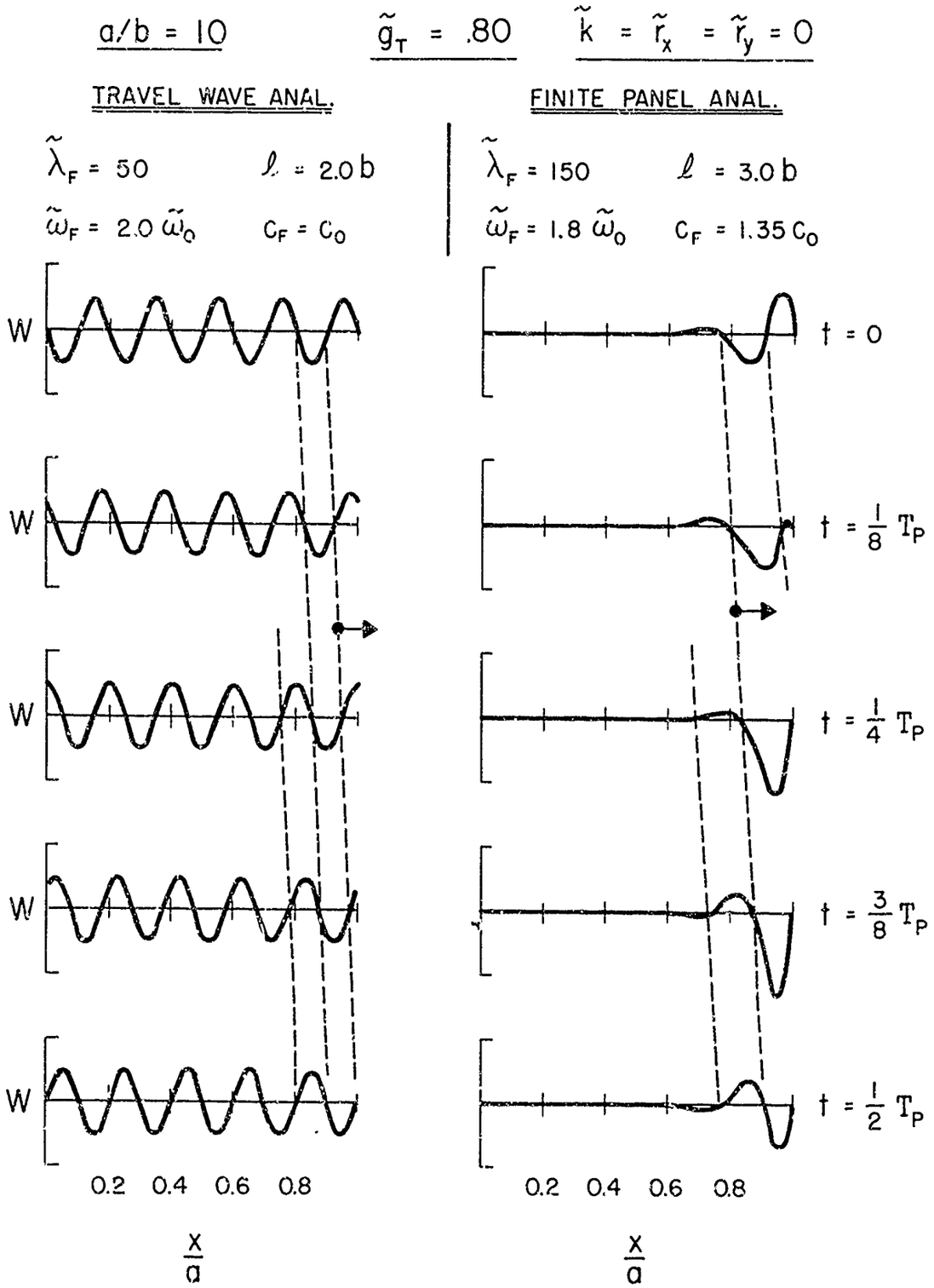

FIG. 20 COMPARISON OF TRAVELING WAVE AND FINITE PANEL ANALYSES -- MODES

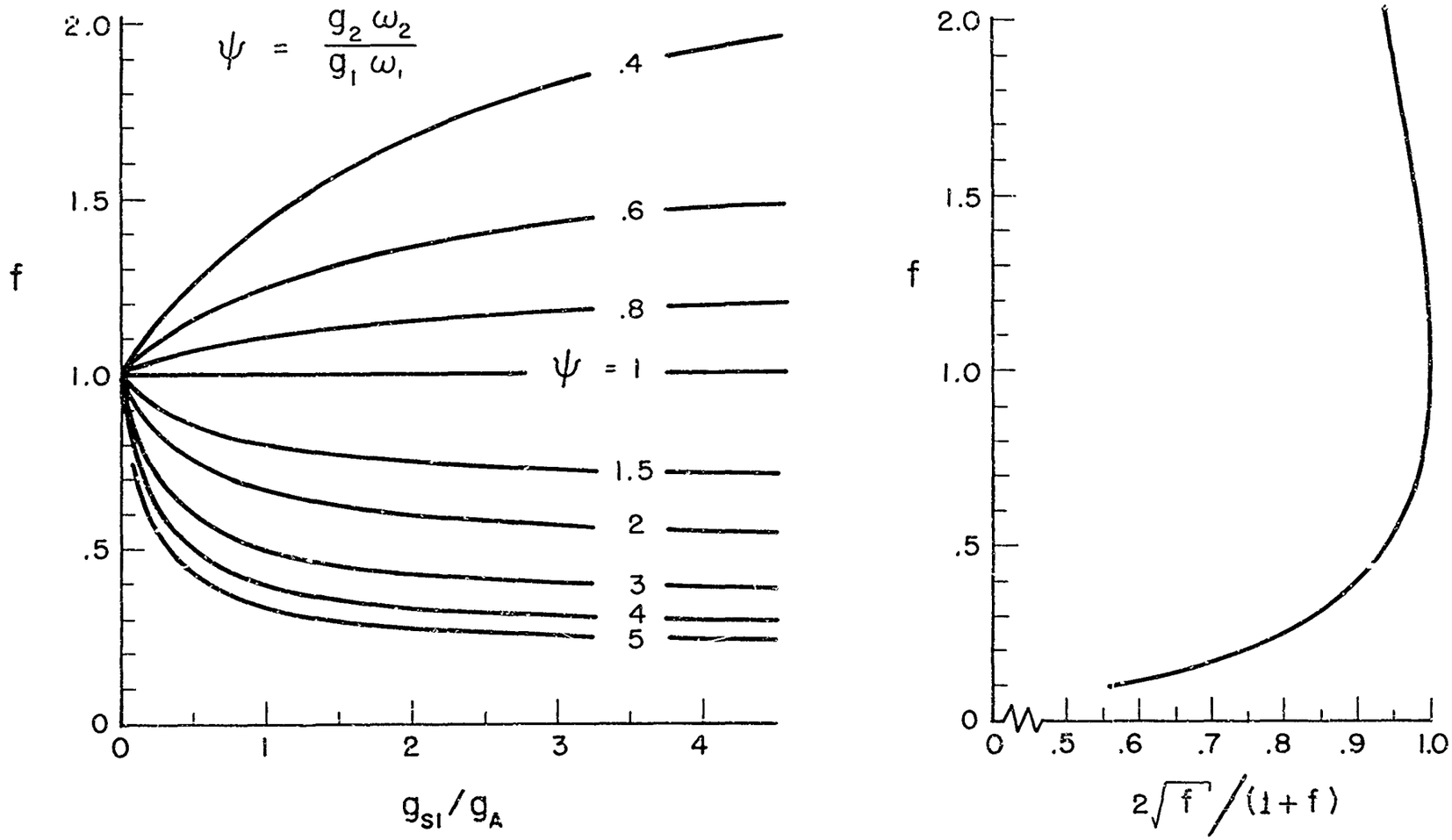

FIG. 21 PARAMETERS FOR UNEQUAL DAMPING

$a/b = k = r_x = r_y = 0$

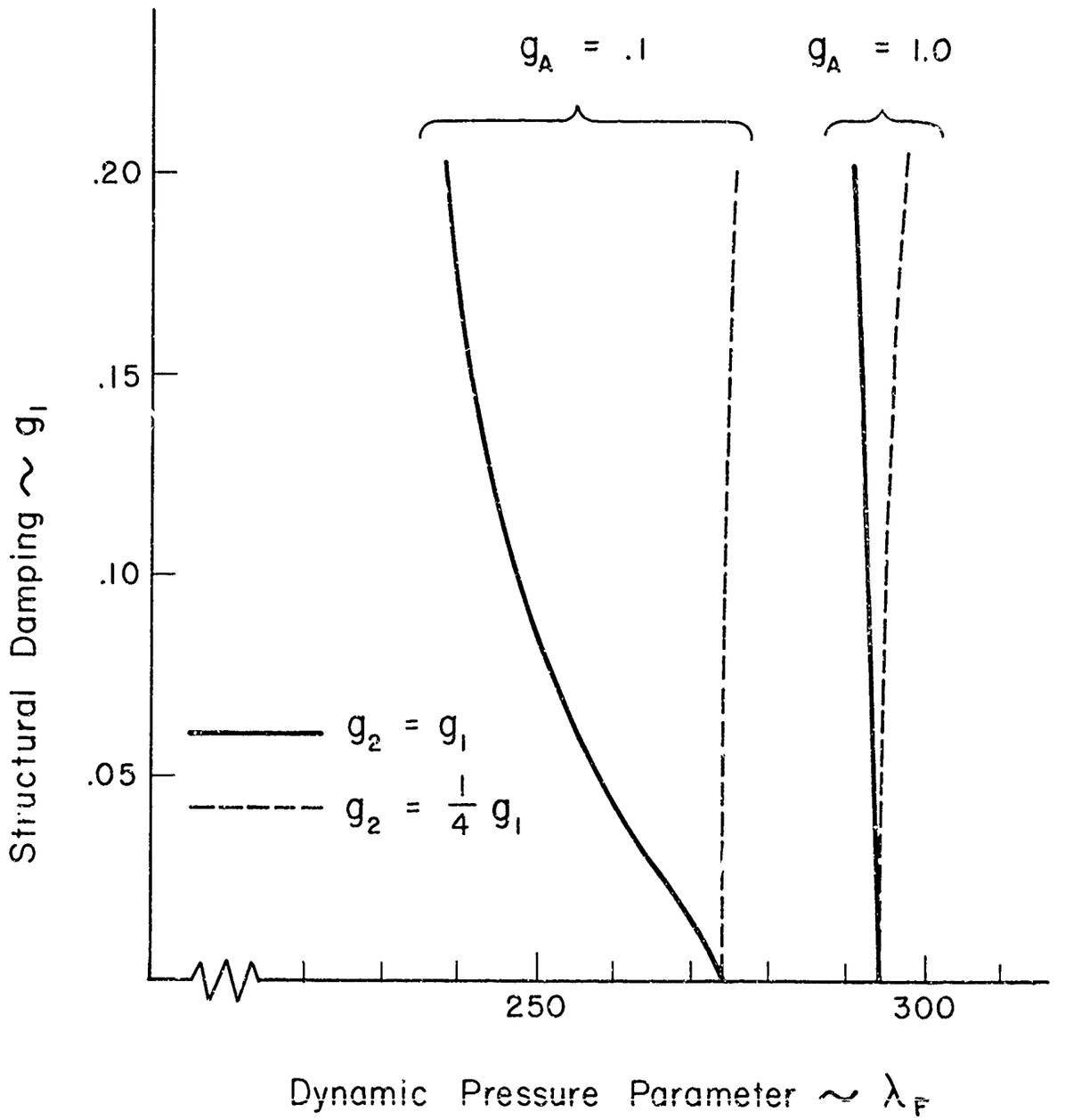

FIG. 22 EFFECT OF STRUCTURAL DAMPING